UNIVERSIDADE FEDERAL DE VIÇOSA

MOAB TORRES DE ANDRADE

UNRAVELING HOW AN AUXIN SIGNALING MUTATION AFFECTS THE XYLEM HYDRAULIC EFFICIENCY AND SAFETY IN TOMATO

VIÇOSA - MINAS GERAIS
2022

MOAB TORRES DE ANDRADE

UNRAVELING HOW AN AUXIN SIGNALING MUTATION AFFECTS THE XYLEM HYDRAULIC EFFICIENCY AND SAFETY IN TOMATO

Thesis submitted to the Plant Physiology Graduate Program of the Universidade Federal de Viçosa in partial fulfillment of the requirements for the degree of *Doctor Scientiae*.

Adviser: Samuel Cordeiro Vitor Martins

Co-advisers: Amanda Ávila Cardoso
Agustin Zsögön

VIÇOSA - MINAS GERAIS
2022

Ficha catalográfica elaborada pela Biblioteca Central da Universidade Federal de Viçosa - Campus Viçosa

T
A553u
2022

Andrade, Moab Torres de, 1992-
Unraveling how an auxin signaling mutation affects the xylem hydraulic efficiency and safety in tomato / Moab Torres de Andrade. – Viçosa, MG, 2022.
1 tese eletrônica (76 f.): il. (algumas color.).

Texto em inglês.
Orientador: Samuel Cordeiro Vitor Martins.
Tese (doutorado) - Universidade Federal de Viçosa, Departamento de Biologia Vegetal, 2022.
Inclui bibliografia.
DOI: https://doi.org/10.47328/ufvbbt.2022.412
Modo de acesso: World Wide Web.

1. Xilema - Anatomia. 2. Tomate - Efeito da auxina. 3. Troca gasosa. 4. *Solanum lycopersicum*. 5. Deficit hídrico. I. Martins, Samuel Cordeiro Vitor, 1986-. II. Universidade Federal de Viçosa. Departamento de Biologia Vegetal. Programa de Pós-Graduação em Fisiologia Vegetal. III. Título.

CDD 22. ed. 575.46

Bibliotecário(a) responsável: Bruna Silva xx

MOAB TORRES DE ANDRADE

UNRAVELING HOW AN AUXIN SIGNALING MUTATION AFFECTS THE XYLEM HYDRAULIC EFFICIENCY AND SAFETY IN TOMATO

Thesis submitted to the Plant Physiology Graduate Program of the Universidade Federal de Viçosa in partial fulfillment of the requirements for the degree of *Doctor Scientiae*.

APPROVED: June 27, 2022.

Assent:

Moab Torres de Andrade
Author

Samuel Cordeiro Vitor Martins
Adviser

To my dear and beloved mother, Maria José Torres de Andrade
(in memoriam).

To my dear grandfather, Abílio Cordeiro da Silva who passed away during this work and I was unable to say goodbye
(in memoriam).

ACKNOWLEDGEMENTS

I first thank God, creator of heaven and earth, for having given me life in such a beautiful and finely adjusted world, which I can examine, besides the book of your words, the book of your works. (*Soli Deo gloria*).

To my friend and mentor professor Samuel C. V. Martins for having accepted to guide me in this journey, for his friendship, valuables teachings, trust, patience, and inspiring personal and professional example of joy and love for knowledge.

To my friend and co-Adviser professor Amanda A. Cardoso for his tireless availability to answer questions, discussion of results and elaboration of analyses, writing tips, for being an example of an admirable scientist who loves science.

To professor Agustin Zsögön thanks for your co-supervision, help in the acquisition of the seeds, in the cultivation and understanding of the tomato mutants.

To professor Fábio M. DaMatta for kindly sharing the laboratory, for his friendship and, in whose name, I thank his entire research group for the companionship and the cups of coffee shared.

To PhD Willian Batista-Silva for the observation of the characteristic, for the willingness to share the research idea.

To the Universidade Federal de Viçosa (UFV), for the opportunity to complete the postgraduate course and all teachers, technicians, and other servers of PPG - Plant Physiology, thank you for teaching and for making this work possible.

To the Coordenação de Aperfeiçoamento de Pessoal de Nível Superior (CAPES), to granting the scholarship.

To my parents, Maria José Torres de Andrade (*in memoriam*) and Cicero Eloi de Andrade, for all the advice, encouragement, and correction that, with God's grace, have striven to teach me the path I should follow in this life.

To my dear sister and second mother, Raquel Torres de Andrade e Lima, for being my psychologist (hahaha) and supporting me with her encouraging words, her warm embrace, her contagious joy, unshakable faith, and her unceasing prayers.

My dear girlfriend Julia S. Oliveira for the strength, care and affection in difficult times, in addition to the exercises and help to make me speak better in public..

To my friends and labmates from Laboratório de Hidráulica de Plantas (LHP): Leonardo (Mr. Capivara; a special thanks to this friend that in this journey became a brother for life), Talitha (Chefa), Eduardo (Dudu), Luciana (Areias), Lizandra, Karoline, Nielson, Mayra, Yara, Carolina, and Aline, for the valuable company, help, laughter, and friendship.

To my friend Guilherme Soares (Dr. Hans Chucrute Soarezenegger), for his dedication and brilliance in saving us when the equipment broke down and for innumerous teachings during the low-cost technical adaptations.

To my brothers from Republica Poligono, Daniel (Cremoso), Bruno (Codózinho), Bruno (Nerso), Ari, and Paulo, thank you for receiving me and for making my time in Viçosa much more joyful and pleasurable, a time that I will treasure in my heart.

To Cal and Prof Cléberson Ribeiro for being so helpful and friendly in providing the benches in the greenhouse for growing tomatoes.

And to everyone who contributed in some way so that this work could happen, which I will not name so as not to be unfair and forget anyone.

To the Brazilian people for funding this work.
My sincere thanks.

“Fides praecedit intellectum; Intellige ut credas crede ut intelligas”.

“*Faith precedes reason; believe in order to understand and understand in order to believe*.”

(St. Augustine of Hippo)

ABSTRACT

ANDRADE, Moab Torres de, D.Sc., Universidade Federal de Viçosa, June, 2022. **Unraveling how an auxin signaling mutation affects the xylem hydraulic efficiency and safety in tomato**. Adviser: Samuel Cordeiro Vitor Martins. Co-advisers: Amanda Ávila Cardoso and Agustin Zsögön.

Auxins are known to regulate xylem development in plants, however, their effects on water transport efficiency and hydraulic safety are poorly known. Here we used tomato plants of the *diageotropica* mutant (*dgt*), which has impaired function of a Cyclophilin 1 *cis*/*trans* isomerase involved in auxin signaling, and its corresponding wild type (WT), to explore its effects on plant hydraulics and leaf gas exchanges. The xylem conduits of *dgt* showed a reduced hydraulically-weighted vessel diameter (D_h) (24-43%) and conduit number (25-58%) in petioles and stems, resulting in lower theoretical hydraulic conductivities (K_t). On the other hand, no changes in root D_h and K_t were observed. In addition, the measured stem and leaf hydraulic conductances of *dgt* agreed with the K_t values and were lower (up to 81%). Despite *dgt* and WT showing similar root D_h and K_t, the measured root hydraulic conductance of *dgt* was 75% lower. The *dgt* mutation increased the vein (D_v) and stomata density (D_s), which could potentially increase photosynthesis. Nevertheless, even presenting the same photosynthetic capacity of WT plants, the *dgt* showed a photosynthetic rate *c.* 25% lower, coupled with a stomatal conductance reduction of 52%. These results clearly demonstrate that increases in D_v and D_s only result in higher leaf gas exchange when accompanied by higher hydraulic efficiency. The *dgt* also showed higher wall thickness per conduit diameter ratio $(t/b)^3$, without major modifications in the pit membranes and cell wall reinforcement. The changes in xylem architecture resulted in a more negative Ψ_{50} (water potential of 50% loss hydraulic conductivity), with a difference of 0.25 MPa and an increase of 64% in hydraulic safety margin comparison with WT plants. Under water deficit, *dgt* took twice as many days to reach Ψ_{50} (-1.34±0.06 MPa) and half the time after rehydration to recover gas exchange when compared with WT (Ψ_{50} = -1.14±0.08 MPa). To confirm that the improved Ψ_{50} of *dgt* was functionally significant, we exposed WT plants to a more intense water deficit (equivalent to *dgt*'s Ψ_{50}) and, indeed, WT plants did not show photosynthetic recovery under this condition. Therefore, we demonstrate that the

changes in the xylem as a function of the mutation in auxin perception result in a severe reduction on in hydraulic efficiency and increased hydraulic safety.

Keywords: Ailsa Craig. Gas exchange. *Solanum lycopersicum.* Water deficit. Water transport. Xylem anatomy.

RESUMO

ANDRADE, Moab Torres de, D.Sc., Universidade Federal de Viçosa, junho de 2022. **Unraveling how an auxin signaling mutation affects the xylem hydraulic efficiency and safety in tomato.** Orientador: Samuel Cordeiro Vitor Martins. Coorientadores: Amanda Ávila Cardoso e Agustin Zsögön.

As auxinas são conhecidas por regular o desenvolvimento do xilema nas plantas, entretanto, seus efeitos sobre a eficiência do transporte de água e segurança hidráulica são pouco conhecidos. Aqui usamos plantas mutantes de tomateiro *diageotropica* (*dgt*), que tem a função prejudicada de uma ciclofilina 1 cis/trans isomerase envolvida na sinalização da auxina, e seu correspondente tipo selvagem (WT), para explorar seus efeitos na hidráulica de plantas e nas trocas de gasosas foliares. O xilema do *dgt* apresentou menor diâmetro de vaso (D_h) (24-43%) e número de condutos (25-58%) em caule e pecíolo, resultando em menores condutividades hidráulicas teóricas (K_t). Por outro lado, não foram observadas alterações de D_h e K_t nas raízes. Além disso, as condutâncias hidráulicas medidas no caule e folha do *dgt* concordaram com os valores de K_t e foram mais baixas (até 81%). Apesar de *dgt* e WT apresentarem D_h e K_t similares nas raízes, a condutância hidráulica da raiz medida no *dgt* foi 75% menor. A mutação *dgt* aumentou a densidade das veias (D_v) e estômatos (D_s), o que potencialmente aumentaria a fotossíntese. No entanto, mesmo apresentando a mesma capacidade fotossintética das plantas WT, o *dgt* mostrou uma taxa fotossintética c. 25% menor, juntamente com uma redução da condutância estomática de 52%. Estes resultados demonstram claramente que os aumentos em D_v e D_s só resultam em maiores taxa de trocas gasosos foliares quando acompanhados de maior eficiência hidráulica. O *dgt* também mostrou maior razão espessura da parede por diâmetro de conduto $(t/b)^3$, sem grandes modificações nas membranas de pontuação e no reforço da parede celular. As mudanças na arquitetura do xilema resultaram em Ψ_{50} (potencial hídrico de 50% de perda de condutividade hidráulica) mais negativos, com uma diferença de 0,25 MPa e um aumento de 64% na margem de segurança hidráulica em comparação com as plantas WT. Sob a seca, a *dgt* levou o dobro dos dias para chegar ao Ψ_{50} (-1,39±0,06 MPa) e metade do tempo após a reidratação para recuperar as trocas gasosas quando comparado com a WT (Ψ_{50}= 1,14±0,08 MPa). Para confirmar que a redução do Ψ_{50} do *dgt* foi funcionalmente

significativo, expusemos as plantas WT a uma seca mais intensa (equivalente ao Ψ_{50} do *dgt*) e, de fato, as plantas WT não mostraram recuperação fotossintética sob esta condição. Portanto, demonstramos que as mudanças no xilema em função da mutação na percepção da auxina resultam em uma redução severa na eficiência hidráulica e no aumento da segurança hidráulica.

Palavras-chave: Ailsa Craig. Anatomia do xilema. Deficit hídrico. *Solanum lycopersicum*. Transporte de água. Trocas de gasosas.

LIST OF FIGURES

CHAPTER 1

CHAPTER 2

LIST OF TABLES

CHAPTER 1

CHAPTER 2

LIST OF ACRONYMS AND ABBREVIATIONS

A_n	Net CO_2 assimilation rates.
A_P	Pit membrane area.
ARF	Auxin response factors.
b	Vessel lumen breadth.
C_{FT}	Leaf capacitance at full turgor.
Crd	*Crispoid* mutant.
C_{TLP}	Leaf capacitance at turgor loss point.
CYP1	Cyclophilin.
dgt	*diageotropica* mutant.
D_{ec}	Epidermal cells density.
D_h	Hydraulic weighted vessel diameter
D_s	Stomatal density.
D_v	Minor vein density.
E	Transpiration rate.
ETR	Electron transport rate.
FAA	Formaldehyde alcohol acetic acid solution.
FOV	Fields of view.
HSM	Hydraulic safety margin.
LA	Leaf area.
LMA	Leaf mass per area unit.
L_s	Stomatal length.
g_m	Mesophyll conductance.
g_s	Stomatal conductance.
K_{leaf}	Leaf hydraulic conductance.
K_{ox}	Outside xylem conductance.
K_{plant}	Whole plant hydraulic conductance.
K_{root}	Root hydraulic conductance.
K_{stem}	Stem hydraulic conductance.
K_t	Theoretical hydraulic conductivity.
K_x	Specific xylem conductance.
PM	Plasma membrane.
PPFD	Photosynthetic photon flux density.

PSII	Photosystem II.
RWC	Relative water content.
RWC_{TLP}	RWC at turgor loss point.
SI	Stomatal index.
t	Cell wall thickness.
V_{cmax}	Maximum carboxylation velocity.
WT	Wild type.
WUE_i	Intrinsic water use efficiency.

LIST OF SYMBOLS

ε	Leaf global modulus of elasticity.
Ψ_{12}	Water potential at 12% cumulative embolism.
Ψ_{50}	Water potential at 50% cumulative embolism.
Ψ_{88}	Water potential at 88% cumulative embolism.
Ψ_{leaf}	Leaf water potential.
Ψ_s	Osmotic potential at full turgor.
Ψ_w	Water Potential.
Ψ_{TLP}	Water potential at turgor loss point.
Φ_{PSII}	Actual quantum yield of photosystem II.

SUMMARY

GENERAL INTRODUCTION

The emergence of tracheophytes, i.e., vascular plants, dates back to 433 million years and the mechanisms behind this event are still under investigation (Silvestro *et al.*, 2015). The development of a vascular system allowed land plants to expand their geographic distribution across the terrestrial environment, with the subsequent emergence of seed plants (373.8 million years) and plants with flowers (143.7 million years; Silvestro et al., 2015). Thus, the large diversity of land plants and other trophic levels now found in the terrestrial biosphere has a strong dependence on the development of the plant vascular system.

The vascular system of plants comprehends xylem and phloem tissues, which play key roles in long-distance transport and have different working mechanisms. The xylem (composed of vessels, tracheids, parenchyma, and fibers) performs mechanical support and the long-distance transport of water and nutrients. The phloem is formed by sieved tube cells, companion cells, and the associated parenchyma. Noteworthy, these tissues work with different pressures: while the phloem operates under positive pressure to distribute photoassimilates from sources to sinks, the xylem operates under tension to transport water and nutrients from the roots to the shoot. The replacement of water lost through leaf transpiration maintain the stomata aperture, which creates a dependence between the photosynthetic activity and the proper functioning of the xylem. Therefore, there is a strong positive relationship between greater water transport efficiency and maximum rates of photosynthesis (Brodribb et al., 2007).

Since water transport in the xylem occurs under tension, in conditions of water deficit and high evaporative demand, leaf water potential might become increasingly negative to the point that the water column is ruptured by seeding of nano air bubbles through the pit membrane in the xylem vessels (Schenk *et al.*, 2015). This process is called cavitation which is followed by the subsequent embolism of the conduit, rendering it unable for water conduction. The tension limit in which cavitation occurs is widely variable among species and it is related to xylem architecture, especially to pit membrane properties. However, the relationship between cavitation and conduit diameter is not well established. Plant hydraulic architecture parameters such as the xylem vulnerability to drought-induced cavitation, specific conductance of plant organs,

and water storage capacity influence plant distribution in different habitats, drought tolerance, and tree mortality (Tyree and Ewers, 1991).

The stem xylem vulnerability to cavitation has received special attention in the last decades due to its potential in predicting tree mortality in drought events. Current evidence shows a strong association between the water potential inducing 50% embolized xylem conduits (Ψ_{50}) in the stem and the lethal water potential for conifers (Brodribb and Cochard, 2009). On the other hand, the threshold water potential for angiosperm mortality is around the level of 88% embolized xylem conduits (Ψ_{88}) (Urli *et al.*, 2013). Given the importance of the hydraulic component in explaining tree mortality (Sevanto *et al.*, 2014; McDowell *et al.*, 2019), it is of utmost importance to unravel the mechanistic basis of how the structure of xylem conduits can determine vulnerability to cavitation. In addition, as these vulnerability parameters were derived from woody plants, it is yet unclear whether they can be applied to herbaceous plants.

As xylem conduits are dead cells at maturity, a large part of the conduit cavitation resistance is determined during their development and differentiation processes. Some structural parameters related to the xylem vulnerability are the average diameter of the conduit (which is extremely determinant in cold-induced cavitation), thickness and porosity of the pit membranes, and depth of the pit chamber (which are characteristics closely related to drought-induced cavitation) (Lens *et al.*, 2011; Gleason *et al.*, 2016). The conduit size is also related to the vulnerability to drought-induced cavitation, being explained by the rare-pit hypothesis mechanism (Christman *et al.*, 2009, 2012). Such a hypothesis proposes that larger conduits have larger pit membrane area and, consequently, are more likely to have a defective membrane with less tension resistance, producing a positive correlation between conduit size and vulnerability (Wheeler *et al.*, 2005; Hacke *et al.*, 2006, 2007; Rockwell *et al.*, 2014).

Most studies that associate hydraulic safety with xylem anatomical properties inferred patterns based on interspecific data (Davis *et al.*, 1999; Hacke *et al.*, 2006; Lens *et al.*, 2011; Gleason *et al.*, 2016; Jacobsen *et al.*, 2019; Liu *et al.*, 2020), making it difficult to isolate the effect of specific variables (for example, the effect of conduit size independently of changes in the pit membrane). Therefore, the hydraulic evaluation of mutant genotypes appears as a promising tool for the understanding of specific changes in hydraulic architecture, i.e., free of major intervening genetic differences. As the formation of xylem conduits occurs during tissue development, an

intrinsic link between plant hydraulics and plant growth regulators should be established. However, from a functional point of view, little is known about the role of hormonal regulation in hydraulic transport efficiency or its vulnerability to cavitation.

The recent development of new non-destructive technologies, such as microCT (Holbrook *et al.*, 2001; Choat *et al.*, 2015) and the optical method (Brodribb et al., 2016), allows the application and assessment of the vulnerability to cavitation in herbaceous plants. Particularly, tomato (*Solanum lycopersicum* L.) is a useful plant model for understanding the relation of phytohormones and hydraulic studies as a myriad of defective mutants in the production, perception of phytohormones are already available. In addition, it has been demonstrated that tomato plants do not exhibit hydraulic vulnerability segmentation (Skelton *et al.*, 2017), which allows the evaluation of cavitation in leaves to be representative of the entire body of the plant. However, as some mutations show very severe phenotypic changes, the challenge is to select genotypes with a changed hydraulic architecture that retains some resemblance with WT plants. As will be described in the next section, we believe the auxin perception mutant *diageotropica* (*dgt*) meets these criteria.

The tomato mutant *dgt* has been recently described with smaller vessel diameters compared to the wild-type (Batista-Silva *et al.*, 2019). As water flow is proportional to the fourth power of conduit radius, according to the Hagen-Poiseuille equation, that should bring significant effects on water transport efficiency (Blackman *et al.*, 2010). At the same time, it can represent changes in the cavitation vulnerability as already described. Therefore, the *dgt* plants provide an opportunity to assess the trade-off between water transport efficiency and safety (Hacke *et al.*, 2006; Gleason *et al.*, 2016), free of considerable “genetic noise”. It is expected that the conduit diameter reduction in *dgt* will result in less hydraulic conductivity together with greater resistance to drought-induced cavitation.

As the knowledge about signaling, regulation of gene expression, and various processes of plant development involving phytohormones are relatively well-known, our study can provide evidence for further biotechnological manipulation aiming at improved xylem efficiency or safety. Thus, this project is an effort to systematically contribute to the understanding of hormonal regulation in plant hydraulics and its future applications.

References

Batista-Silva W, Medeiros DB, Rodrigues-Salvador A, *et al.* 2019. Modulation of auxin signalling through DIAGETROPICA and ENTIRE differentially affects tomato plant growth via changes in photosynthetic and mitochondrial metabolism. Plant Cell and Environment **42**, 448–465.

Blackman CJ, Brodribb TJ, Jordan GJ. 2010. Leaf hydraulic vulnerability is related to conduit dimensions and drought resistance across a diverse range of woody angiosperms. New Phytologist **188**, 1113–1123.

Brodribb TJ, Cochard H. 2009. Hydraulic failure defines the recovery and point of death in water-stressed conifers. Plant Physiology **149**, 575–584.

Brodribb TJ, Feild TS, Jordan GJ. 2007. Leaf maximum photosynthetic rate and venation are linked by hydraulics. Plant Physiology **144**, 1890–1898.

Brodribb TJ, Skelton RP, Mcadam SAM, Bienaimé D, Lucani CJ, Marmottant P. 2016. Visual quantification of embolism reveals leaf vulnerability to hydraulic failure. New Phytologist **209**, 1403–1409.

Choat B, Brodersen CR, Mcelrone AJ. 2015. Synchrotron X-ray microtomography of xylem embolism in Sequoia sempervirens saplings during cycles of drought and recovery. New Phytologist **205**, 1095–1105.

Christman MA, Sperry JS, Adler FR. 2009. Testing the ‘rare pit’ hypothesis for xylem cavitation resistance in three species of Acer. New Phytologist **182**, 664–674.

Christman MA, Sperry JS, Smith DD. 2012. Rare pits, large vessels and extreme vulnerability to cavitation in a ring-porous tree species. New Phytologist **193**, 713–720.

Davis SD, Sperry JS, Hacke UG. 1999. The relationship between xylem conduit diameter and cavitation caused by freezing. American Journal of Botany **86**, 1367–1372.

Gleason SM, Westoby M, Jansen S, *et al.* 2016. Weak tradeoff between xylem safety and xylem-specific hydraulic efficiency across the world's woody plant species. New Phytologist **209**, 123–136.

Hacke UG, Sperry JS, Feild TS, Sano Y, Sikkema EH, Pittermann J. 2007. Water transport in vesselless angiosperms: Conducting efficiency and cavitation safety. International Journal of Plant Sciences **168**, 1113–1126.

Hacke UG, Sperry JS, Wheeler JK, Castro L. 2006. Scaling of angiosperm xylem structure with safety and efficiency. Tree Physiology **26**, 689–701.

Holbrook NM, Ahrens ET, Burns MJ, Zwieniecki MA. 2001. In vivo observation of cavitation and embolism repair using magnetic resonance imaging. Plant Physiology **126**, 27–31.

Jacobsen AL, Brandon Pratt R, Venturas MD, Hacke UG. 2019. Large volume vessels are vulnerable to water-stress-induced embolism in stems of poplar. IAWA Journal **40**, 4–22.

Lens F, Sperry JS, Christman MA, Choat B, Rabaey D, Jansen S. 2011. Testing hypotheses that link wood anatomy to cavitation resistance and hydraulic conductivity in the genus Acer. New Phytologist **190**, 709–723.

Liu H, Ye Q, Gleason SM, He P, Yin D. 2020. Weak tradeoff between xylem hydraulic efficiency and safety: climatic seasonality matters. New Phytologist.

McDowell NG, Brodribb TJ, Nardini A. 2019. Hydraulics in the 21st century. New Phytologist **224**, 537–542.

Rockwell FE, Wheeler JK, Holbrook NM. 2014. Cavitation and its discontents: Opportunities for resolving current controversies. Plant Physiology **164**, 1649–1660.

Schenk HJ, Steppe K, Jansen S. 2015. Nanobubbles: A new paradigm for air-seeding in xylem. Trends in Plant Science **20**, 199–205.

Sevanto S, Mcdowell NG, Dickman LT, Pangle R, Pockman WT. 2014. How do trees die? A test of the hydraulic failure and carbon starvation hypotheses. Plant, Cell and Environment **37**, 153–161.

Silvestro D, Cascales-Miñana B, Bacon CD, Antonelli A. 2015. Revisiting the origin and diversification of vascular plants through a comprehensive Bayesian analysis of the fossil record. New Phytologist **207**, 425–436.

Skelton RP, Brodribb TJ, Choat B. 2017. Casting light on xylem vulnerability in an herbaceous species reveals a lack of segmentation. New Phytologist **214**, 561–569.

Tyree MT, Ewers FW. 1991. The hydraulic architecture of trees and other woody plants. New Phytologist **119**, 345–360.

Urli M, Porté AJ, Cochard H, Guengant Y, Burlett R, Delzon S. 2013. Xylem embolism threshold for catastrophic hydraulic failure in angiosperm trees. Tree Physiology **33**, 672–683.

Wheeler JK, Sperry JS, Hacke UG, Hoang N. 2005. Inter-vessel pitting and cavitation in woody Rosaceae and other vessel led plants: A basis for a safety versus efficiency trade-off in xylem transport. Plant, Cell and Environment **28**, 800–812.

CHAPTER 1

Impaired auxin signaling increases vein and stomatal density but reduces hydraulic efficiency and ultimately net photosynthesis

Moab T. Andrade, Leonardo A. Oliveira, Talitha S. Pereira, Amanda A. Cardoso, Willian Batista-Silva, Fábio M. DaMatta, Agustín Zsögön[1] Samuel C. V. Martins

Already published in: https://doi.org/10.1093/jxb/erac119

Introduction

The foliar CO_2 uptake and water vapor loss to the atmosphere share a common gateway, namely, the stomata. Stomata can impose a considerable limitation to the CO_2 diffusion, and species with greater stomatal conductance (g_s), which is defined by density, size, and aperture of stomata, often exhibit higher net CO_2 assimilation rates (A_n) (Lawson and Blatt, 2014). Thus, increasing the number of stomata per area (i.e. stomatal density; D_s) has been a key target for improving g_s and hence A_n in several crop species (Tanaka *et al.*, 2013; Lawson and Blatt, 2014; Franks *et al.*, 2015).

Despite displaying high D_s, leaves can still exhibit low g_s due to stomatal closure if the water lost through transpiration exceeds the capacity of the plant's internal water supply system. This supply system comprises all the components involved in water acquisition, transport, and loss, and its efficiency is measured by the plant hydraulic conductance (K_{plant}) (Brodribb and Feild, 2000; Tyree and Zimmermann, 2002; Sack and Scoffoni, 2013). The K_{plant}, in turn, is determined by the sum of the hydraulic resistances of roots, stem, and leaves, with leaves constituting an important bottleneck of the hydraulic path (Sack and Holbrook, 2006). It has been demonstrated, for instance, that leaves exhibiting greater K_{leaf} achieve higher rates of g_s and hence A_n (Brodribb *et al.*, 2007; McAdam *et al.*, 2017). Notably, the xylem network has an important role in defining K_{leaf} so that a high vein density (D_v) frequently results in higher K_{leaf} and, ultimately, in potentially higher A_n (Sack and Holbrook, 2006; Sack and Scoffoni, 2013; Carins Murphy *et al.*, 2016; McAdam *et al.*, 2017). Moreover, the fossil record show a coevolution and coordination of D_v and D_s emphasizing that a higher vulnerability to desiccation (given by higher D_s) takes place unless an improved water transport system (given by higher D_v) is developed (De Boer *et al.*, 2012; Brodribb *et*

al., 2013). Both D_s (which directly impacts maximum g_s and therefore A_n) and D_v (which is related to water supply) decline with increases in leaf expansion through a passive dilution mechanism across several plant species (Carins Murphy *et al.*, 2012, 2014, 2016). Leaf expansion is determined by external and internal factors, but, among the internal ones, the phytohormone auxin has been demonstrated to directly impact leaf expansion (the acid growth hypothesis) (Du *et al.*, 2020); therefore, it is possible that this hormone also acts to indirectly modulate D_s and D_v via such passive dilution mechanism.

Besides modulating foliar cell expansion, auxin has been observed to directly regulate stomatal and vein differentiation. Indeed, evidence suggests auxin as a negative regulator of stomatal development (Balcerowicz and Hoecker, 2014); however, at some level, polar auxin transport (PAT) also appears to have an important positive regulatory role given that mutations in PAT negatively affect stomatal differentiation (Mayer *et al.*, 1993; Spitzer *et al.*, 2009). Regarding the leaf vein development, auxin transport mediated by PIN-FORMED (PIN) efflux carriers creates “auxin maxima” that determines the polarity and induces cell differentiation into strands pattern, according to the "auxin-flow canalization hypothesis" (Sachs, 1981, 1991; Aloni, 2013; Růžička *et al.*, 2015; Carins Murphy *et al.*, 2017). Furthermore, an auxin link governing leaf venation and the photosynthetic rate was established in *Pisum sativum* by McAdam et al. (2017), who characterized the mutation at the *Crispoid* (*Crd*) locus, known for encoding a key enzyme of the YUCCA family (involved in auxin biosynthesis) (Mashiguchi *et al.*, 2011). This mutation alters the auxin homeostasis during leaf development, resulting in reduced D_v and, consequently, lower K_{leaf} and A_n.

This set of evidence shows that changes in auxin activity can modulate hydraulic aspects and stomatal parameters, which, in turn, would impact photosynthetic capacity. The tomato mutant *diageotropica* (*dgt*) has impaired function in a cyclophilin 1 protein (CYP1) which catalyzes the *cis-trans* isomerization of peptidyl-prolyl bonds in target proteins (Oh *et al.*, 2006), including those of the Auxin/Indole-3-Acetic Acid (Aux/IAA) family (Jing *et al.*, 2015). Aux/IAA proteins are repressors of the auxin response through interaction with the transcription factors (TFs) of the ARF family. CYP1 activity acts by facilitating the Aux/IAA proteasomal degradation and, when CYP1 loss its function, Aux/IAA are not degraded and ARF TFs become continually repressed. As a result, this impairment in the auxing signaling cascade characterizes *dgt* by reduced sensitivity to auxin. Furthermore, DGT affects PAT in tomato

(Ivanchenko *et al.*, 2015) and it has been recently shown that the *dgt* mutant has smaller xylem vessel diameters when compared to the wild type (WT) (Batista-Silva *et al.*, 2019). The Hagen-Poiseuille equation predicts that decreases in xylem diameter should bring significant effects on the xylem water transport efficiency as the maximum potential water flow would be proportional to the fourth power of conduit radius (Blackman *et al.*, 2010). On the other hand, empirical evidence suggests that the contribution of large-diameter xylem vessels might be oversized because of the presence of transverse pressure gradients that redirect water flow from wide to narrow vessels (Bouda *et al.*, 2019). In any case, the xylem changes resulting from *dgt* mutation provide an exciting opportunity to assess the effect of changes in xylem vessel diameter on plant hydraulics efficiency.

Here we used plants of *dgt* and its WT to determine how an impaired auxin signaling affects xylem and stomata development and, consequently, impact plant hydraulic conductance and leaf gas exchange. Specifically, we tested (i) whether a reduction in auxin perception would result in higher D_s and D_v due to a lower passive dilution or whether it would decrease D_v due to the direct effect of auxin in leaf vein formation; (ii) whether changes in size and density of xylem conduits would impact hydraulic conductances throughout the plant and (iii) whether the leaf phenotype resulted from a reduced perception in auxin would affect leaf gas exchanges. Our results show that the impaired CYP1-mediated auxin signaling bring strong reduction on hydraulic efficiency transport resulting in a negative impact on net photosynthesis, despite increases in leaf vein and stomatal density. Thus, the investigation of the auxin role on water transport, g_s and A_n might open an important avenue for biotechnological engineering.

Materials and methods

Plant material

Plants of *dgt* and its WT (background Ailsa Craig) (Oh *et al.*, 2006) were cultivated from seeds in a greenhouse in Viçosa (20° 45' 37" S 42° 52' 04" W), Brazil. Seeds were sown in a commercial substrate (Tropstrato HT®), and, upon appearance of the first true leaf, the seedlings were transplanted into 5 L pots (one individual per pot) containing the same substrate until they were approximately two-month-old. Conditions in the greenhouse during the day were *c.* 1500 µmol m^{-2} s^{-1} of maximum

photosynthetic photon flux density (PPFD), photoperiod around 12 h, 25.2 to 31.9°C, and 46 to 64% of relative humidity. Plants were weekly fertilized (around 2 g per plant) using a commercial NPK formulation (10:10:10).

Morphology and anatomy of roots, stems, and leaves

The leaf area (LA) was measured using a flatbed scanner and analyzed with ImageJ (National Institutes of Health, Bethesda, USA). The same leaves (n = 8) were dried in a forced-air oven for 48 h at 70°C and weighted using a precision digital balance to determine the dry weight and calculate the leaf mass per area unit (LMA) The roots were scanned with EPSON LA2400 Perfection V700/V750 scanner equipped with additional light (transparency unit) at a resolution of 400 dpi. The tips number was measured using the WinRhizo software (Bouma *et al.*, 2000).

For cross-sections, samples (n = 6) were taken from the median portion of roots, stems, and terminal petioles. Petioles were sampled from the apical leaflet of completely expanded leaves inserted in the middle third of shoots. Samples were fixed in FAA for 48 h (Johansen, 1940) and maintained in 70% ethanol in water (v/v) for further analyses. They were next dehydrated in a graded ethanol series and embedding according to the manufacturer's instructions (Leica Historesin embedding kit, Leica Microsystems, Heidelberg, Germany). Sections (5-μm-thin) were obtained with an automatic rotary microtome (Leica RM 2155, Leica Microsystems Inc., Deerfield, USA), transferred to glass slides, stained with toluidine blue (O'Brien *et al.*, 1964), and mounted in Permount® resin. Paradermal sections of two adjacent leaflets from the same leaf previously utilized for cross-sections were utilized for D_s and D_v analyses. Samples taken from the middle portion of the leaves avoiding the midrib were cleared in 100% methanol for 48 h at ambient temperature, followed by incubation in 95% lactic acid at 90°C until full clarification.

For each sample, five fields of view (FOV) at 4× magnification (for D_v measurements), three FOV at 10× magnification (for mesophyll measurements), and 10 FOV at 20× magnification [for D_s, stomatal length (L_s), and stomatal index (SI; obtained by the ratio: stomatal number / epidermal cells number)] were taken using a digital camera (Zeiss AxioCam HRc, Göttinger, Germany) mounted on a light microscope (AX70 TRF, Olympus Optical, Tokyo, Japan). Measurements were performed using Image-Pro Plus 4.5 (Media Cybernetics, Silver Spring, USA). D_v was measured as the total length of leaf vascular tissue (second and lower vein orders) and

D_s as the total number of stomata per mm^2 of leaf area. For roots, stems and petioles, the area of functional xylem (A), hydraulically weighted diameter of xylem conduits (D_h), theoretical axial hydraulic conductance (K_t) were calculated assuming a elliptic form using the following equations (Lewis and Boose, 1995; Martins *et al.*, 2014):

$$A = \sum \frac{\pi ab}{4}$$

$$D_h \cong \sqrt{\frac{2a^1b^2}{a^2 + b^2}}$$

$$K_t = \sum \frac{[\pi a^3 b^3]}{64\eta(a^2b^2)}$$

where a and b are the short and long vessel lumen breadth, and η is the viscosity of water at 25°C.

Plant hydraulics and leaf gas exchange

The maximum leaf hydraulic conductance (K_{leaf}) was determined through the evaporative flux method (Sack *et al.*, 2002; Brodribb and Holbrook, 2006). From 08h00 to 16h00, completely expanded leaves (n = 9) had their petioles cut under water and their entire leaf blades placed inside a leaf conifer chamber (LI-6400-18 RGB Light Source, LI-COR, Lincoln, USA) connected to a LI-6400XT (LI-COR, Lincoln, USA). Conditions within the leaf cuvette were: 1000 µmol m^{-2} s^{-1} PPFD (10% of blue light), 400 µmol CO_2 mol^{-1} air, and vapor pressure deficit at approximately 1.0 kPa. The transpiration rate (E) was logged following maximum stability in leaf gas exchange (after c. 30 min). Leaves were then removed from the chamber, bagged for c. 15 min (to allow leaf equilibration), and had their water potential (Ψ_{leaf}) measured with a Scholander pressure chamber (Model 1000, PMS Instruments, Albany, USA). After that, the leaves were scanned and measured using ImageJ (National Institutes of Health, Bethesda, USA). Finally, E was normalized by leaf area and K_{leaf} was calculated as

$$K_{leaf} = -E/\ \Psi_{leaf}.$$

The root and stem hydraulic conductance (K_{root} and K_{stem}) were measured using an adapted method using a pressure chamber (Sperry *et al.*, 1988; Miyamoto *et al.*, 2001). Plants (c. 50-day-old) were hydrated and equilibrated in a glass bell jar for 30 min or until guttation, in the dark. Then a stem section (14.6 ± 0.6 cm) was cut immediately above ground, the leaves were cut and the stem section was immersed

in a 50 ml falcon tube containing ultrapure water type 1 (Millipore Synergy ™ Ultrapure Water Purification System, Millipore, France). Next, the stem was placed inside a Scholander pressure chamber describe above and connected to a water-filled silicone tube coupled to a precision digital balance (AY 220 model, Shimadzu, Japan). Increasing pressures were applied to the chamber (0.01, 0.02, 0.03, 0.04, and 0.05 MPa) and the flow generated (g s^{-1}) was recorded every 30 s during 150 s. The conductance (mmol m^{-2} s^{-1} MPa^{-1}) was derived from the slope of the flow rate line versus pressure MPa and normalized by the total leaf area. The estimate of the whole plant hydraulic conductance (K_{plant}) was made by summing the inverse of the measured conductances

$$1/K_{plant} = 1/K_{root} + 1/K_{stem} + 1/K_{leaf}).$$

K_{plant} was also measured according to the evaporative flux method (Tsuda and Tyree, 2000) by evaluating the predawn and midday Ψ_{leaf} and the gravimetric *E*, measuring the mass of the pots in the same time (6 h period).

Leaf gas exchange was measured using a gas-exchange system equipped with an integrated fluorescence chamber head (area: 2 cm^2; LI-6400XT, LI-COR, Lincoln, USA). Measurements were taken on fully expanded leaves (n = 5) in the middle third of the plant between 09h00 and 11h00 (VPD 1.7 ± 0.14 kPa; T_{air} 30.4 ± 0.71 °C). Conditions in the chamber were the same utilized for K_{leaf} measurements. After reaching the steady state, net CO_2 assimilation rate (A_n), stomatal conductance to water vapor (g_s) and transpiration rate (E) were recorded. In light-adapted leaves, the actual quantum yield of photosystem II Φ_{PSII} was determined according to the procedures of Genty *et al.* (1989) and the electron transport rate (ETR) was then calculated as:

$$ETR = \alpha\beta \text{ PPFD } \Phi_{PSII}$$

where PPFD is the photosynthetically active photon flux density, α is the leaf absorptance and β is the PSII optical cross section. The Intrinsic water use efficiency (WUE_i) was calculated as A_n/g_s from measurements made between 09h00 and 11h00 (VPD 1.7 ± 0.14 kPa; T_{air} 30.4 ± 0.71 °C). To estimate the maximum carboxylation velocity (V_{cmax}) by the single point method, A_n and C_i obtained in the measurements described above were used, in addition to values of respiration in the dark (R_d). R_d was measured on leaves previously acclimated for 30 minutes in the dark. Subsequently, V_{cmax} was calculated as described by De Kauwe et al. (2016).

Statistical analysis

Morphological, anatomical, and physiological traits between the two genotypes were compared by unpaired Student's t-tests ($\alpha < 0.05$). Statistical analyses and the graphs were generated using GraphPad Prism 8.0 (GraphPad Software, San Diego, USA).

Results

Alterations in plant morphology and anatomy

The *dgt* mutants were consistently smaller than the WT, with reduced cross-section areas of stems (c. 73%) and petioles (c. 66%) and increased cross-section area of roots (c. 53%); the area of functional xylem followed the changes in cross-section areas, decreasing in stems and petioles, and increasing in roots (Fig. 1A-B;Table 1). Leaves showed lower LMA and exhibited higher D_s (65 and 63% for abaxial and adaxial leaf sides) with slightly lower guard cell length (13 and 11%) and similar SI in the *dgt* when compared to the WT (Table 1 and Fig. 2A-C). Finally, leaves of the *dgt* also exhibited higher D_v (49%, Fig. 2D). The higher D_s and D_v observed for the *dgt* leaves were accompanied by decreases in leaf area; in addition, D_s and D_v were positively correlated with each other (Fig. 3A-C).

Hydraulic conductances and leaf gas exchange

Roots of the *dgt* showed similar Dh, a higher number of xylem conduits, and similar K_t compared with the WT (Fig. 1C-E). Conversely, stems and petioles of the *dgt* exhibited reduced D_h, a lower number of xylem conduits, and, as a result, a lower K_t relative to the WT (Fig. 1C-E). Within the plant, D_h values of stem and petioles were similar, but higher than root D_h in WT; on the other hand, in *dgt*, D_h values of roots, petioles and stem were all the same (Fig. 1C). Regarding hydraulic conductances, the *dgt* mutant showed considerably lower maximum conductances of roots, stems, and leaves (by 75, 80, and 18%, respectively) as well as lower estimated and measured K_{plant} (Table 1). Leaf gas exchange (A_n , g_s and E) was also significantly reduced in the *dgt* compared with their WT counterparts (Fig. 4A-D). The g_s was nearly halved in the *dgt*, while A_n decreased by 24%. The higher declines in g_s than in A_n resulted in higher WUE_i in the *dgt* over the WT plants. Also, the Ψ_{leaf} was consistently lower during the

day for *dgt* than WT plants (Fig. 3E). Finally, there was no significant difference for the V_{cmax} on a C_i basis between *dgt* and WT plants (Fig. 4A).

Discussion

The dgt mutation alters the xylem anatomy and hydraulic efficiency

The auxin signaling impairment mediated by the *dgt* mutation caused severe effects on the hydraulic architecture of tomato plants. The analyses of xylem conduits showed a reduced D_h and conduit number in stem and terminal petioles, resulting in lower K_t for these organs (Fig. 1C-E). Interestingly, this pattern was not observed in roots, where the *dgt* and WT presented similar Dh and K_t, with *dgt* producing a higher conduit number than the WT. Such an increase in conduit redundancy might be a compensation for the impairment in lateral root formation observed in *dgt* (Ivanchenko *et al.*, 2015) (Fig. S1A-B). Consistent with our findings, Silva *et al.* (2018) analyzed the interaction of *SELF-PRUNING* and *DGT* genes in the development and growth form in the Micro-Tom background and also observed that the *dgt* showed a smaller vessel size. Taken together, the reduction of D_h and a lower number of conduits suggest an important role of auxin in the formation and radial expansion of early vessel cells. This role is believed to be mediated by cyclophilin 1 (CYP1, encoded by *DGT* gene in tomato), which was previously described as cytosolic protein (Gasser *et al.*, 1990). Recent evidence suggests that CYP1 is involved in the long-distance regulation of shoot gravitropism, which reinforces the possibility that CYP1 is also involved in xylem development, however its specific role is yet unclear (Spiegelman *et al.*, 2020). Since hypocotyl segments of *dgt* have impairment in the induction and negative regulation of plasma membrane (PM) H^+ ATPases in response to applied auxin (Coenen *et al.*, 2002) we speculate that the reduction of D_h is a consequence of an impaired cell wall acidification. Our rationale follows the classical growth model which advocates an essential role of PM H^+-ATPases to promote apoplast acidification, cell wall modification, and further cell expansion by turgor pressure (Arsuffi and Braybrook, 2018). In addition to an impaired cell wall acidification, another contributing factor for the reduced expansion would be the possibility that *dgt* cells operate with lower turgor pressure. Accordingly, we indeed observed a lower Ψ_{leaf} (difference of 0.26 MPa at midday) in *dgt* during the day (Fig. 3E). Therefore, it is possible that *dgt* plants

simultaneously experience lower turgor pressure and impaired acidification of the cell wall.

The changes in hydraulic conductance measured along the whole plant followed the theoretically predicted by K_t for stem and leaves. However, the K_{root} observed for *dgt* (75% lower than for WT) diverged from root K_t (which was similar to WT). This may be related to sampling the median region of the principal root for the anatomical analysis: *dgt* mutants have a pronounced primary root with high caliber whereas WT plants show a high number of roots with similar caliber (Fig. S1A). This contrasting result highlights the importance of measuring the effective hydraulic conductance to complement the analysis of $K_{t,}$ which is based only on anatomical data (Fig. S2). Interestingly, the change in K_{leaf} was lower compared with the changes in K_{root} and K_{stem}, which may be associated with adjustments in the outside xylem component of water transport through leaf mesophyll termed K_{ox} (Scoffoni *et al.*, 2017). To overcome the severe reductions in D_h (43% lower) and K_t (91% lower), which, in theory, affect especially the xylem component (K_x), changes in K_{ox} would have been of greater relevance to maintain K_{leaf} at a proper magnitude for stomatal opening and CO_2 uptake. The outside-xylem pathway is extremely complex and involves multiple tissues, but some K_{ox} related leaf structural traits may have contributed to facilitating the water movement through the leaf such as the highest D_v and lower mesophyll intercell airspaces of *dgt*. The higher D_v implies a higher occurrence of bundle sheath cells, which are less hydraulically resistive (Buckley *et al.*, 2015; Zsögön *et al.*, 2015). On other hand, the lower mesophyll intercellular airspace (Fig. S3B) would result in higher connectivity between cells (Scoffoni *et al.*, 2017; Xiong and Nadal, 2020). In addition, the highest D_v, D_s and lower thickness (Fig. S3B) presented by *dgt* leaves might have contributed to the maintenance of K_{leaf} since all these variables reduce the pathway for water transport from xylem terminals to stomata.

Altogether, the analysis of the effective hydraulic efficiencies of the different plant organs showed that, although hydraulically limited as a whole, the main bottleneck for water transport in *dgt* was located in the root system. This result implies a severe effect of *dgt* mutation on the hydraulic efficiency, which was evident by the considerably lower K_{plant} and the consistent Ψ_{leaf} reduction during the day in *dgt* when compared with the WT (Table 1; Fig. 3E). It seems that the compromised capacity to produce large xylem vessels in the whole plant, as noted by the similar D_h and $D_{h\ max}$ in all organs of *dgt* (Table S1), might have had a role in this reduced hydraulic

efficiency. Interestingly, Brodribb *et al.* (2013) discuss that, if mutations in cell size do not produce parallel changes in all cell lines in the leaf, the critical link between water supply and photosynthesis is likely to be lost, which seems to be the case in *dgt* plants.

We also speculate that the increased D_h of root xylem could be a hydraulic compensation to overcome the reduced organogenesis of lateral root primordium, but how could this condition lead to an increased D_h of root xylem whereas the opposite (reduced D_h) was observed in the remaining plant parts remains unknown.

Despite exhibiting higher stomatal and vein density, the *dgt* mutants still achieve lower leaf gas exchange

Another structural change observed in the *dgt* was a greater D_v and D_s when compared with the WT. Given that the genotypes presented a similar stomatal index, the changes in D_s are unlikely to have been resulted from a higher differentiation frequency. In fact, changes in D_s and D_v likely occurred due to a passive dilution effect driven by changes in the rate of epidermal cell expansion (Carins Murphy *et al.*, 2014, 2016). Different from the observed in *Crispoid* (a defective auxin biosynthetic mutant), which presents a significant reduction in leaf vein formation (McAdam *et al.*, 2017), the *dgt* mutation did not affect the vein production in leaves and, instead, increased the number of veins and stomata per area.

It is well established that increases in D_v and D_s tend to favor higher A_n. D_v is a trait associated with water distribution efficiency and correlates positively with higher A_n in the foliage of a diverse group of plants, from mosses to angiosperms (Brodribb *et al.*, 2007). Likewise, it has been reported an enhancement of 30% in leaf photosynthetic capacity in transgenic *Arabidopsis* plants with 350% increased D_s (Tanaka *et al.*, 2013). Taken together, these observations would suggest a higher A_n in the *dgt*; however, the *dgt* showed both lower A_n (25%) and g_s (52%) than WT, resulting in a 55% higher WUE_i (Fig. 4D). Noteworthy, once LMA show intraspecifically covariation with photosynthetic capacity, it would be expected a lower A_n in *dgt* mutants given their reduced LMA (Table 1) (Poorter et al., 2009); however, LMA is not directly linked with photosynthesis and has its effect explained by another latent variable, like cell number, volume or constituents (Shipley et al., 2006). Indeed, *dgt* shows a higher cell number per area of leaf cross-section and overall smaller cells than WT, which indicates that mesophyll cells were not replaced by veins and the low LMA may be a result of a reduced inherent growth rate (Poorter et al., 2009). Furthermore, the

photosynthetic capacity (as measured by V_{cmax} (Fig. 4A) and the electron transport rate (Fig. S1C) was similar between *dgt* and WT, implying that the lower A_n was solely a consequence of diffusive limitations. Such limitations could be due to a lower mesophyll and/or stomatal conductances, but, as Batista-Silva *et al.* (2019) found similar mesophyll CO_2 conductance (g_m) in *dgt* and WT plants, and, considering that a lower gm would also be seen as a lower V_{cmax} (which was not the case), we contend on the predominance of stomatal limitations in *dgt*.

Such a decrease in g_s suggests that the impairment of water supply (through a reduction in K_{plant}) might have counteracted the increases in D_v and D_s. We also do not discard that the more negative water potential could have led to a higher production of abscisic acid (ABA) in *dgt;* in fact, around midday, water potential would have been close to the turgor loss point (Table S1), which is currently accepted as the trigger for major increments in foliar ABA (Cardoso *et al.*, 2020*b*). Interestingly, from midday onwards, the decreasing difference in leaf water potential between WT and *dgt* might be due to further decreases in leaf transpiration which alleviates xylem tension in *dgt*. Finally, our data suggest that, in a water restricted environment, the *dgt* genotype has a competitive advantage (due to the high WUE_i) and that controlled biotechnological changes in conduits diameter may be a valid approach to achieve improvements in WUE in crops under water-limited scenarios.

Conclusion

In summary, our study shows the first in-depth hydraulic characterization of the effects of the reduced auxin signaling mediated by *DGT*. We found considerable changes in xylem anatomy, i.e., reduction in conduits number and diameter (in stems and leaves), which resulted in severe impacts on hydraulic efficiency at the whole-plant level. In particular, our analysis identified the roots as the hydraulic bottleneck of *dgt* which was associated with the impairment of secondary root primordium initiation shown by this genotype. Curiously, unlike what was observed in the *dgt* stem and petiole, there was an increased xylem conduit production in roots which might be a compensatory mechanism for the loss of hydraulic efficiency. Despite the increases in D_v and D_s, which would theoretically increase A_n, A_n was still lower in *dgt*, likely due to a limited water transport capacity. Despite the reduction in LMA, the *dgt* mutant shows similar V_{cmax}, indicating that photosynthetic capacity was not altered. The lower K_{plant}

resulted in lower g_s, highlighting the crucial role of water transport efficiency in determining the maximum photosynthetic rates. Also, we found evidence that *DGT*, an auxin response mediator, plays a relevant role in proper xylem conduit development with strong implications on hydraulic efficiency. Our study shows that the understanding of the nature of the auxin-hydraulic relation might be a pathway to crop improvements in face of environmental changes.

References

Aloni R. 2013. Role of hormones in controlling vascular differentiation and the mechanism of lateral root initiation. Planta **238**, 819–830.

Arsuffi G, Braybrook SA. 2018. Acid growth: An ongoing trip. Journal of Experimental Botany **69**, 137–146.

Balcerowicz M, Hoecker U. 2014. Auxin - a novel regulator of stomata differentiation. Trends in Plant Science **19**, 747–749.

Batista-Silva W, Medeiros DB, Rodrigues-Salvador A, *et al.* 2019. Modulation of auxin signalling through DIAGETROPICA and ENTIRE differentially affects tomato plant growth via changes in photosynthetic and mitochondrial metabolism. Plant Cell and Environment **42**, 448–465.

Blackman CJ, Brodribb TJ, Jordan GJ. 2010. Leaf hydraulic vulnerability is related to conduit dimensions and drought resistance across a diverse range of woody angiosperms. New Phytologist **188**, 1113–1123.

De Boer HJ, Eppinga MB, Wassen MJ, Dekker SC. 2012. A critical transition in leaf evolution facilitated the Cretaceous angiosperm revolution. Nature Communications **3**.

Bouda M, Windt CW, McElrone AJ, Brodersen CR. 2019. In vivo pressure gradient heterogeneity increases flow contribution of small diameter vessels in grapevine. Nature Communications **10**.

Bouma TJ, Nielsen KL, Koutstaal B. 2000. Sample preparation and scanning protocol for computerised analysis of root length and diameter. Plant and Soil **218**, 185–196.

Brodribb TJ, Feild TS. 2000. Stem hydraulic supply is linked to leaf photosynthetic capacity: Evidence from New Caledonian and Tasmanian rainforests. Plant, Cell and Environment **23**, 1381–1388.

Brodribb TJ, Feild TS, Jordan GJ. 2007. Leaf maximum photosynthetic rate and venation are linked by hydraulics. Plant Physiology **144**, 1890–1898.

Brodribb TJ, Holbrook NM. 2006. Declining hydraulic efficiency as transpiring leaves desiccate: Two types of response. Plant, Cell and Environment **29**, 2205–2215.

Brodribb TJ, Jordan GJ, Carpenter RJ. 2013. Unified changes in cell size permit coordinated leaf evolution. New Phytologist **199**, 559–570.

Buckley TN, John GP, Scoffoni C, Sack L. 2015. How does leaf anatomy influence

water transport outside the xylem? Plant Physiology **168**, 1616–1635.

Cardoso AA, Gori A, Da-Silva CJ, Brunetti C. 2020. Abscisic acid biosynthesis and signaling in plants: Key targets to improve water use efficiency and drought tolerance. Applied Sciences (Switzerland) **10**.

Carins Murphy MR, Dow GJ, Jordan GJ, Brodribb TJ. 2017. Vein density is independent of epidermal cell size in Arabidopsis mutants. Functional Plant Biology **44**, 410–418.

Carins Murphy MR, Jordan GJ, Brodribb TJ. 2012. Differential leaf expansion can enable hydraulic acclimation to sun and shade. Plant, Cell and Environment **35**, 1407–1418.

Carins Murphy MR, Jordan GJ, Brodribb TJ. 2014. Acclimation to humidity modifies the link between leaf size and the density of veins and stomata. Plant, Cell and Environment **37**, 124–131.

Carins Murphy MR, Jordan GJ, Brodribb TJ. 2016. Cell expansion not cell differentiation predominantly co-ordinates veins and stomata within and among herbs and woody angiosperms grown under sun and shade. Annals of Botany **118**, 1127–1138.

Coenen C, Bierfreund N, Lüthen H, Neuhaus G. 2002. Developmental regulation of H+-ATPase-dependent auxin responses in the diageotropica mutant of tomato (*Lycopersicon esculentum*). Physiologia Plantarum **114**, 461–471.

Du M, Spalding EP, Gray WM. 2020. Rapid Auxin-Mediated Cell Expansion. Annual Review of Plant Biology **71**, 379-402.

Franks PJ, W. Doheny-Adams T, Britton-Harper ZJ, Gray JE. 2015. Increasing water-use efficiency directly through genetic manipulation of stomatal density. New Phytologist **207**, 188–195.

Gasser CS, Gunning DA, Budelier KA, Brown SM. 1990. Structure and expression of cytosolic cyclophilin/peptidyl-prolyl cis-trans isomerase of higher plants and production of active tomato cyclophilin in *Escherichia coli*. Proceedings of the National Academy of Sciences of the United States of America **87**, 9519–9523.

Genty B, Briantais JM, Baker NR. 1989. The relationship between the quantum yield of photosynthetic electron transport and quenching of chlorophyll fluorescence. Biochimica et Biophysica Acta - General Subjects **990**, 87–92.

Ivanchenko MG, Zhu J, Wang B, *et al.* 2015. The cyclophilin a DIAGEOTROPICA gene affects auxin transport in both root and shoot to control lateral root formation.

Development (Cambridge) **142**, 712–721.

Jing H, Yang X, Zhang J, *et al.* 2015. Peptidyl-prolyl isomerization targets rice Aux/IAAs for proteasomal degradation during auxin signalling. Nature Communications **6**, 1–10.

Johansen DA. 1940. *Plant microtechnique*. London: McGraw-Hill Book Company, Inc.

De Kauwe MG, Lin Y, Wright IJ, *et al.* 2016. A test of the 'one-point method' for estimating maximum carboxylation capacity from field-measured, light-saturated photosynthesis. New Phytologist **210**, 1130–1144.

Lawson T, Blatt MR. 2014. Stomatal size, speed, and responsiveness impact on photosynthesis and water use efficiency. Plant Physiology **164**, 1556–1570.

Lewis AM, Boose ER. 1995. Estimating volume flow rates through xylem conduits. American Journal of Botany **82**, 1112–1116.

Martins SCV, Galmés J, Cavatte PC, Pereira LF, Ventrella MC, DaMatta FM. 2014. Understanding the low photosynthetic rates of sun and shade coffee leaves: Bridging the gap on the relative roles of hydraulic, diffusive and biochemical constraints to photosynthesis. PLoS ONE **9**, 1–10.

Mashiguchi K, Tanaka K, Sakai T, *et al.* 2011. The main auxin biosynthesis pathway in *Arabidopsis*. Proceedings of the National Academy of Sciences of the United States of America **108**, 18512–18517.

Mayer U, Buttner G, Jurgens G. 1993. Apical-basal pattern formation in the Arabidopsis embryo: Studies on the role of the gnom gene. Development **117**, 149–162.

McAdam SAM, Eléouët MP, Best M, *et al.* 2017. Linking auxin with photosynthetic rate via leaf venation. Plant Physiology **175**, 351–360.

Miyamoto N, Steudle E, Hirasawa T, Lafitte R. 2001. Hydraulic conductivity of rice roots Naoko. Journal of experimental botany **52**, 1835–1846.

O'Brien TP, Feder N, McCully ME. 1964. Polyehromatic Staining of Plant Cell Walls by Toluidine Blue O. Protoplasma **59**, 1–8.

Oh KC, Ivanchenko MG, White TJ, Lomax TL. 2006. The *diageotropica* gene of tomato encodes a cyclophilin: A novel player in auxin signaling. Planta **224**, 133–144.

Růžička K, Ursache R, Hejátko J, Helariutta Y. 2015. Xylem development–from the cradle to the grave. New Phytologist, 207(3), 519-535..pdf. New Phytologist **207**, 519–535.

Sachs T. 1981. The Control of the Patterned Differentiation of Vascular Tissues.

Advances in Botanical Research **9**, 151–262.

Sachs T. 1991. Cell polarity and tissue patterning in plants. Development **112**, 83–93.

Sack L, Holbrook NM. 2006. Leaf hydraulics. Annual Review of Plant Biology **57**, 361–381.

Sack L, Melcher PJ, Zwieniecki MA, Holbrook NM. 2002. The hydraulic conductance of the angiosperm leaf lamina: a comparison of three measurement methods. Journal of Experimental Botany **53**, 2177–2184.

Sack L, Scoffoni C. 2013. Leaf venation : structure , function , development , evolution , ecology and. New Phytologist **198**, 983–1000.

Scoffoni C, Albuquerque C, Brodersen CR, Townes S V., John GP, Bartlett MK, Buckley TN, McElrone AJ, Sack L. 2017. Outside-xylem vulnerability, not Xylem embolism, controls leaf hydraulic decline during dehydration. Plant Physiology **173**, 1197–1210.

Silva WB, Vicente MH, Robledo JM, Reartes DS, Ferrari RC, Bianchetti R, Araújo WL, Freschi L, Peres LEP, Zsögön A. 2018. Self-pruning acts synergistically with diageotropica to guide auxin responses and proper. Plant Physiology **176**, 2904–2916.

Sperry JS, Donnelly JR, Tyree MT. 1988. A method for measuring hydraulic conductivity and embolism in xylem. Plant, Cell & Environment **11**, 35–40.

Spiegelman Z, Broshi O, Shahar A, Omer S, Hak H, Wolf S. 2020. Long-distance regulation of shoot gravitropism by Cyclophilin 1 in tomato (Solanum lycopersicum) plants. Planta **252**, 1–10.

Spitzer C, Reyes FC, Buono R, Sliwinski MK, Haas TJ, Otegui MS. 2009. The ESCRT-Related CHMP1A and B proteins mediate multivesicular body sorting of auxin carriers in Arabidopsis and are required for plant development. Plant Cell **21**, 749–766.

Tanaka Y, Sugano SS, Shimada T, Hara-Nishimura I. 2013. Enhancement of leaf photosynthetic capacity through increased stomatal density in Arabidopsis. New Phytologist **198**, 757–764.

Tsuda M, Tyree MT. 2000. Plant hydraulic conductance measured by the high pressure flow meter in crop plants. Journal of Experimental Botany **51**, 823–828.

Tyree MT, Zimmermann MH. 2002. *Xylem Structure and the Ascent of Sap*. Berlin: Springer Berlin Heidelberg.

Xiong D, Nadal M. 2020. Linking water relations and hydraulics with photosynthesis. Plant Journal **101**, 800–815.

Zsögön A, Alves Negrini AC, Peres LEP, Nguyen HT, Ball MC. 2015. A mutation that eliminates bundle sheath extensions reduces leaf hydraulic conductance, stomatal conductance and assimilation rates in tomato (*Solanum lycopersicum*). New Phytologist **205**, 618–626.

Tables and Figures

Table 1. Leaf area (LA), leaf mass per area unit (LMA), stomatal density (D_s), stomatal length (L_s), epidermal cells density (D_{ec}), leaf hydraulic conductance (K_{leaf}), stem hydraulic conductance (K_{stem}), root hydraulic conductance (K_{root}), and estimated and measured whole plant hydraulic conductance (K_{plant}) for two genotypes of tomato plants, i.e. WT and the *dgt*. Data are means ± SE (n = 6).

Traits	WT	*dgt*
LA (cm^2)	33.15 ± 1.34	23.56 ± 1.64**
LMA (g m^{-2})	27.65 ±2.19	22.00 ±1.37*
$D_{s\ adaxial}$ (mm^{-2})	78.41 ±6.92	129.66 ±11.31**
$D_{s\ abaxial}$ (mm^{-2})	163.92 ±13.23	267.32 ±18.72**
$L_{s\ adaxial}$ (μm)	35.25 ±0.80	30.62 ±0.35**
$L_{s\ abaxial}$ (μm)	30.98 ±0.61	27.30 ±0.35**
$D_{ec\ adaxial}$ (mm^{-2})	289.42 ±28.55	452.53 ±46.79**
$D_{ec\ abaxial}$ (mm^{-2})	325.41 ±43.06	531.43 ±42.03**
K_{leaf} (mmol m^{-2} s^{-1} MPa^{-1})	14.32 ±0.35	11.80 ±0.65**
K_{stem} (mmol m^{-2} s^{-1} MPa^{-1})	68.15 ± 13.85	13.40 ± 0.86**
K_{root} (mmol m^{-2} s^{-1} MPa^{-1})	15.32 ± 1.04	3.80 ± 0.61**
$K_{plant\ estimated}$ (mmol m^{-2} s^{-1} MPa^{-1})	6.37 ± 0.25	2.28 ± 0.41**
$K_{plant\ measured}$ (mmol m^{-2} s^{-1} MPa^{-1})	5.05 ± 0.49	3.92 ± 0.13*

Asterisks indicate significant genotypic differences according to Student's t test (^{ns} = not significant, * = $P < 0.05$, ** = $P < 0$.

Fig. 1. (A) Representative images of 50-day-old plants of tomato from two genotypes, i.e. WT and the *dgt* mutant; (B) Representative cross-sectional images of roots, stems and petioles of WT (above) and *dgt* (below) mutant plants (data shown are the functional xylem area: x10^3 μm^2) ; (C) hydraulically weighted diameter of xylem conduits, (D) xylem conduit number and (E) theoretical hydraulic conductivity (K_t) of roots, stems and petioles for two genotypes of tomato plants, i.e. WT and the *dgt*. Data are means ± SE. The symbol + in boxplot are means. c= cortex; p= pith; ph= phloem; x= xylem.

Fig. 2. (A) Stomatal density, (B) guard cell length, (C) stomatal index and (D) minor vein density of plants of tomato from two genotypes, i.e. WT and *dgt*. Representative images of stomatal distribution (scale bar = 50 μm), stomatal size (scale bar = 10 μm)

and leaf venation (scale bar = 300 μm) are depicted in (A), (B), and (C) respectively. Bars are means ± SE (n=6). Symbols associated with bars are individual points. Asterisks indicate significant change between genotypes according to Student's t test. ns = not significant. ** = P < 0.01.

Fig. 3. Relationships between (A) stomatal density and 1/leaf area, (B) vein density and 1/√leaf area and (C) vein and stomatal density (D) hydraulically weighted diameter of xylem conduits, (E) time course of leaf water potential (Ψ_{leaf}) for two genotypes of tomato plants, i.e. WT and the *dgt*. PD = Predawn leaf water potential. Data are means ± SE. Continuous lines represent regressions and dashed lines indicate the 95% confidence interval. Pearson correlation coefficients (R) and significance levels (*P*) for each regression are shown. Bars are means ± SE (n=6). Symbols associated with bars are individual points. Asterisks indicate significant differences between genotypes according to Student's *t* test (^{ns} = not significant, ** = P < 0.01).

Fig. 4. (A) Net CO_2 assimilation rate (*A*), (B) stomatal conductance to water vapor (g_s), (C) transpiration rate (*E*), (D) the intrinsic water use efficiency (WUE_i), (E) scheme of the *diageotropica* mutation of auxin perception results in a significant reduction in water transport efficiency (i.e., hydraulic conductances: K_{root}, K_{stem} and K_{leaf}), which counteract the positive effect of increased minor vein density (D_v) and stomatal density (D_s), showing the priority of the water transport function in the regulation of gas exchange parameters in tomato plants. Data are means ± SE (*n* = 6). Asterisks indicate significant genotypic differences according to Student's *t* test (* = P < 0.05, * = P < 0.05, ** = P < 0.01.

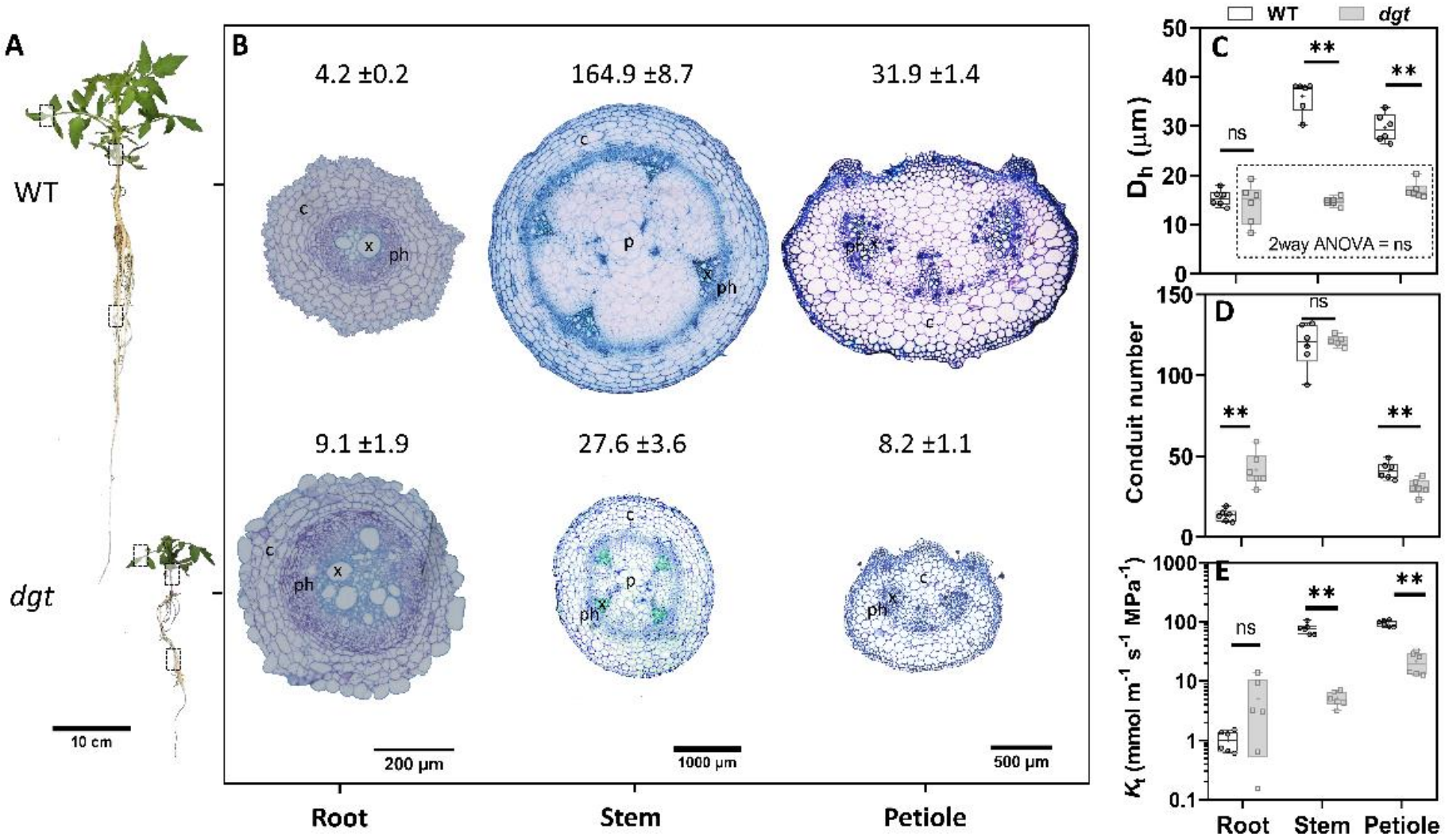
A
WT
dgt
10 cm
B
4.2 ±0.2
164.9 ±8.7
31.9 ±1.4
9.1 ±1.9
27.6 ±3.6
8.2 ±1.1
c
x
ph
p
200 µm
1000 µm
500 µm
Root
Stem
Petiole
WT
dgt
C
D
E
ns
**
2way ANOVA = ns
Dh (µm)
Conduit number
Kt (mmol m-1 s-1 MPa-1)

Figure 1.

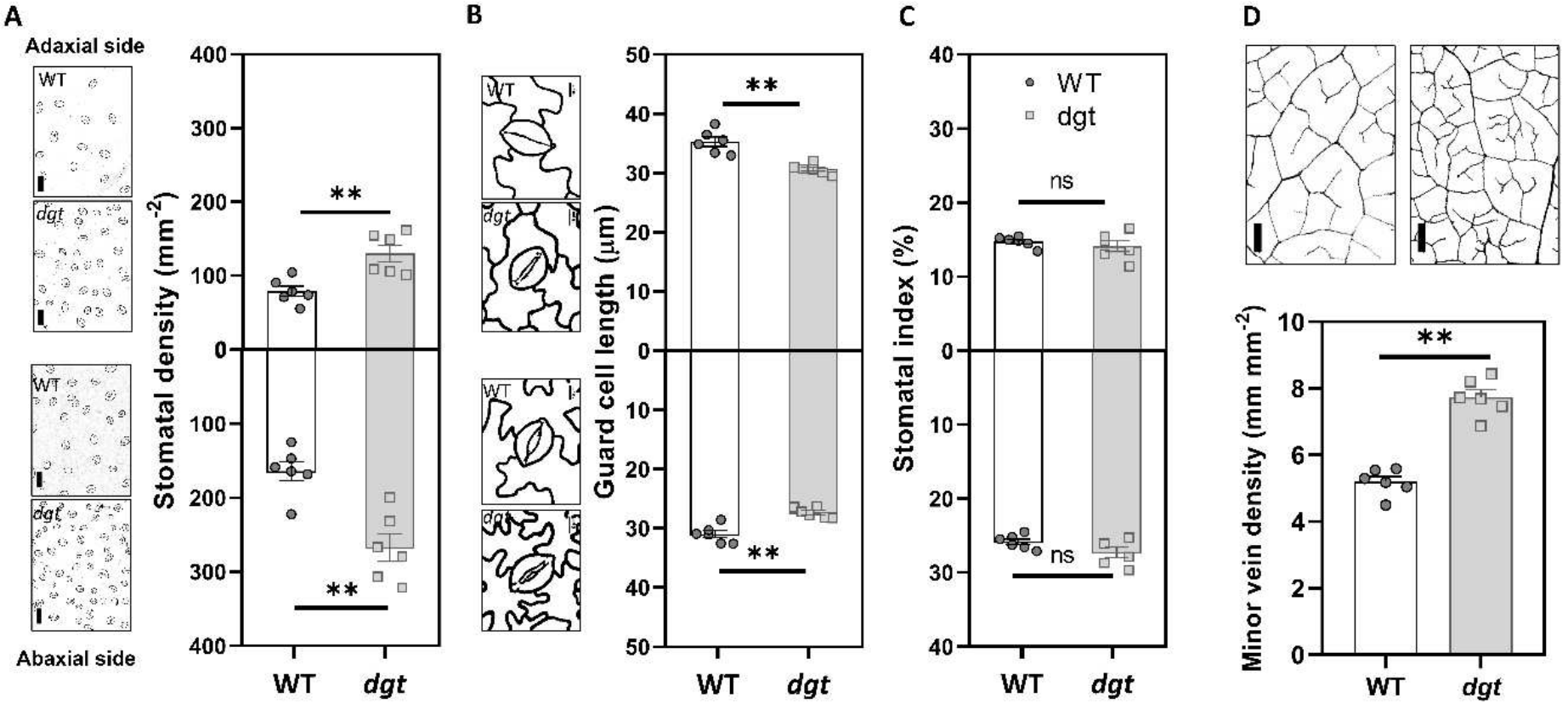
A
Adaxial side
WT
dgt
WT
dgt
Abaxial side
Stomatal density (mm-2)
400
300
200
100
0
100
200
300
400
**
**
WT
dgt
B
WT
dgt
WT
dgt
Guard cell length (μm)
50
40
30
20
10
0
10
20
30
40
50
**
**
WT
dgt
C
WT
dgt
Stomatal index (%)
40
30
20
10
0
10
20
30
40
ns
ns
WT
dgt
D
Minor vein density (mm mm-2)
10
8
6
4
2
0
**
WT
dgt

Figure 2.

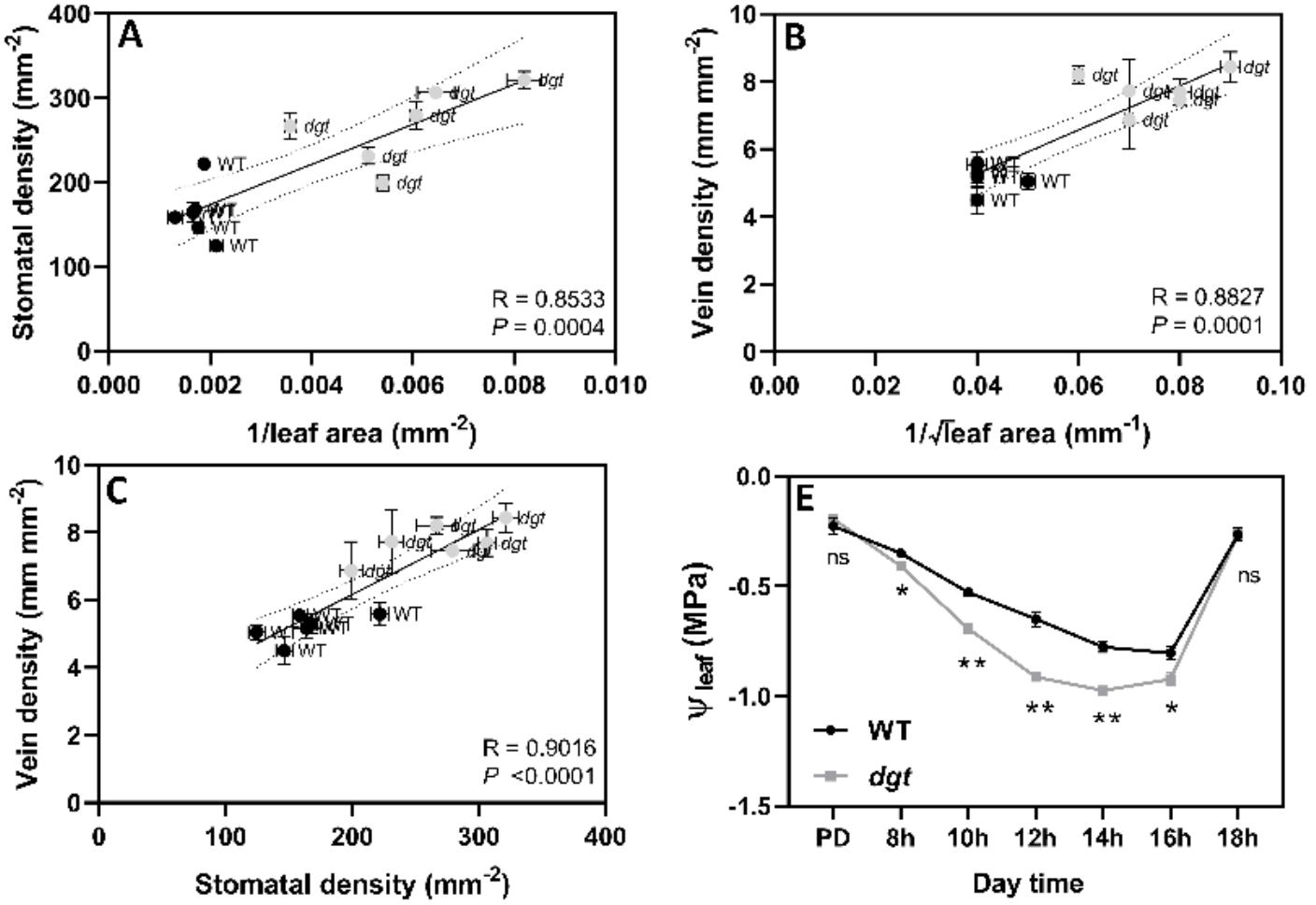
A
Stomatal density (mm-2)
1/leaf area (mm-2)
R = 0.8533
P = 0.0004
WT
dgt
B
Vein density (mm mm-2)
1/√leaf area (mm-1)
R = 0.8827
P = 0.0001
C
Vein density (mm mm-2)
Stomatal density (mm-2)
R = 0.9016
P <0.0001
E
Ψ leaf (MPa)
ns
*
**
WT
dgt
PD
8h
10h
12h
14h
16h
18h
Day time

Figure 3.

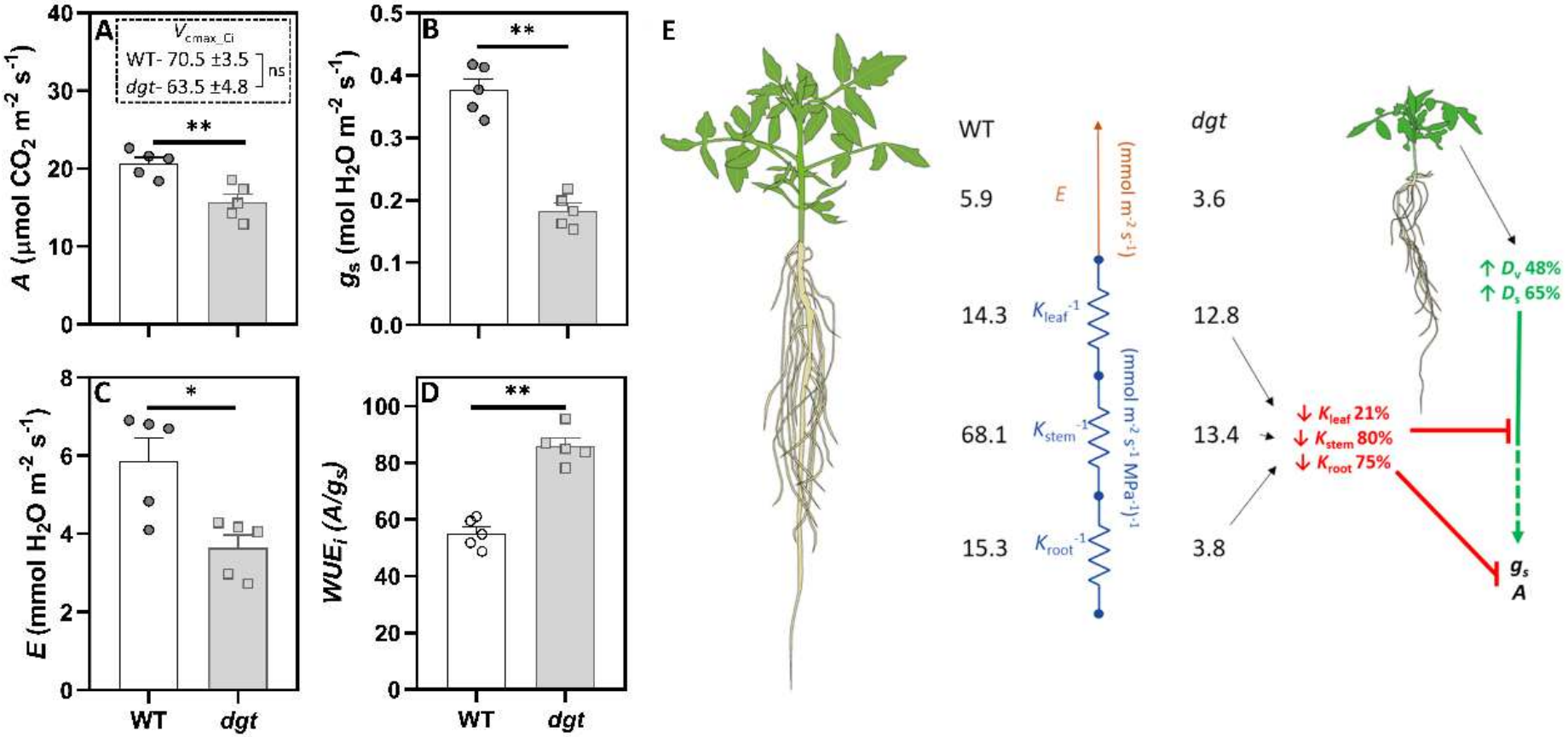
A
V_{cmax_Ci}
WT- 70.5 ±3.5
dgt- 63.5 ±4.8
ns
**
A (µmol CO2 m-2 s-1)
B
**
gs (mol H2O m-2 s-1)
C
*
E (mmol H2O m-2 s-1)
D
**
WUEi (A/gs)
WT
dgt
E
WT
5.9
E
(mmol m-2 s-1)
14.3
Kleaf-1
68.1
Kstem-1
15.3
Kroot-1
(mmol m-2 s-1 MPa-1)-1
dgt
3.6
12.8
13.4
3.8
↓ Kleaf 21%
↓ Kstem 80%
↓ Kroot 75%
↑ Dv 48%
↑ Ds 65%
gs
A

Figure 4.

Supplementary material

Table S1. Saturated water content (SWC), water potential at the turgor loss point (Ψ_{TLP}), osmotic potential at full turgor (Ψ_s), relative water content at the turgor loss point (RWC_{TLP}), global modulus of elasticity (ε), capacitance at full turgor (C_{FT}), capacitance at the turgor loss point (C_{TLP}), leaf cuticular conductance (g_{min}), hydraulically weighted diameter of xylem conduits (D_h), maximum hydraulically weighted diameter ($D_{h\ max}$), hydraulically weighted diameter median ($D_{h\ median}$), xylem conduit number and xylem area for two genotypes of tomato plants, i.e. WT and the *dgt* mutant, in its respective plant organs. Data are means ± SE (n = 6).

Water relations Traits	**WT**	***dgt***	
SWC (g g^{-1})	7.55 ± 0.37	7.24 ± 0.17^{ns}	LEAF
Ψ_{TLP} (-MPa)	0.81 ± 0.04	0.88 ± 0.02^{ns}	
Ψs (-MPa)	0.70 ± 0.04	0.76 ± 0.02^{ns}	
RWC_{TLP} (%)	90.11 ± 0.08	86.25 ±0.97**	
ε (MPa)	7.10 ± 0.84	6.86 ± 0.39^{ns}	
C_{FT} (mol m^{-2} MPa^{-1})	1.17 ±0.05	1.03 ± 0.07^{ns}	
C_{TLP} (mol m^{-2} MPa^{-1})	3.19 ± 0.30	3.34 ± 0.46^{ns}	
g_{min} (mmol m^{-2} s^{-1})	1.69 ± 0.18	1.60 ± 0.11^{ns}	
Vessel xylem traits	- - - - -	- - - - -	
D_h (μm)	15.36 ± 0.67	14.18 ± 1.66^{ns}	ROOT
$D_{h\ max}$ (μm)	52.22 ± 2.77	36.77 ± 5.38*	
$D_{h\ median}$ (μm)	11.38 ± 0.40	11.40 ± 1.21^{ns}	
Number	13.33 ± 1.48	41.33 ± 4.35**	
Xylem area (%)	4.05 ±0.15	11.70 ±2.86*	
D_h (μm)	36.06 ± 1.32	13.85 ± 0.35**	STEM
$D_{h\ max}$ (μm)	98.29 ± 2.63	31.54 ± 2.04**	
$D_{h\ median}$ (μm)	31.04 ± 1.94	13.85 ± 0.41**	
Number	118.50 ± 5.74	138.33 ± 17.17^{ns}	
Xylem area (%)	3.81 ±0.33	3.19 ±0.21^{ns}	
D_h (μm)	29.63 ± 1.28	16.98 ± 068**	PETIOLE
$D_{h\ max}$ (μm)	48.58 ± 1.79	27.81 ± 1.21**	
$D_{h\ median}$ (μm)	30.14 ± 1.28	16.75 ± 0.96**	
Number	41.00 ± 2.14	30.67 ± 2.06**	

Asterisks indicate significant genotypic differences according to Student's t test (^{ns} = not significant, * = $P < 0.05$, ** = $P < 0.01$).

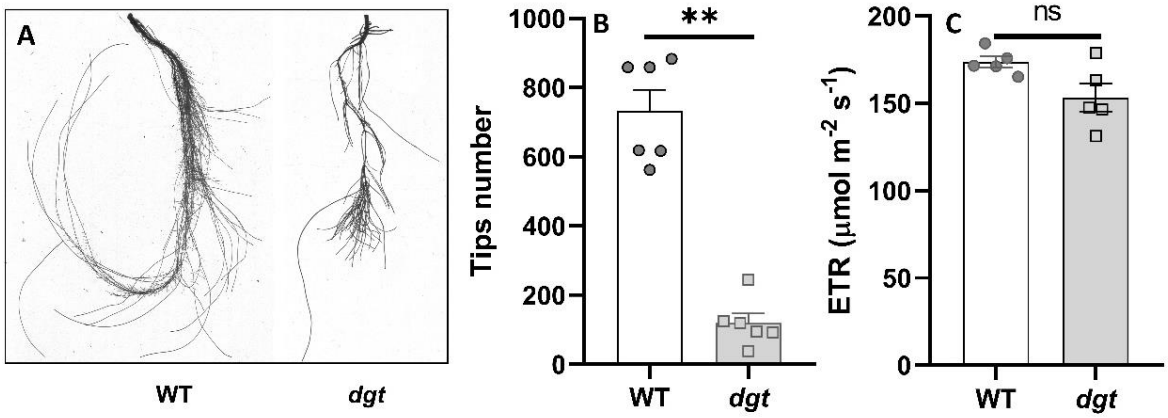

Fig. S1. (A) Representative image of the root system obtained by the WinRhizo, (B) root tip number and (C) electron transport rate (ETR) for two genotypes of tomato plants, i.e. WT and the *dgt* mutant. Bars are mean ± SE (n = 6). Symbols associated with bars are individual points. Asterisks indicate significant difference between genotypes according to Student's t test (^{ns} = not significant, ** = P < 0.01).

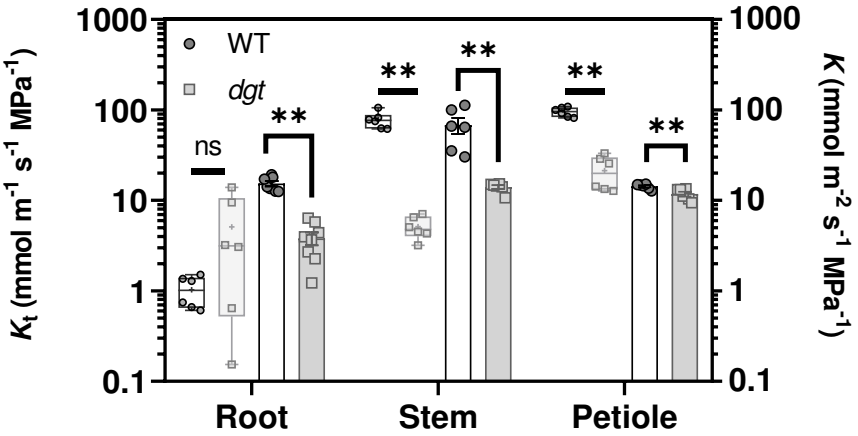

Fig. S2. Theoretical hydraulic conductivity (boxplot) and measured hydraulic conductance (bars) of roots, stems and petioles/leaf for two genotypes of tomato plants, i.e. WT and the *dgt*. Data are means ± SE. The symbols + in boxplot are means.

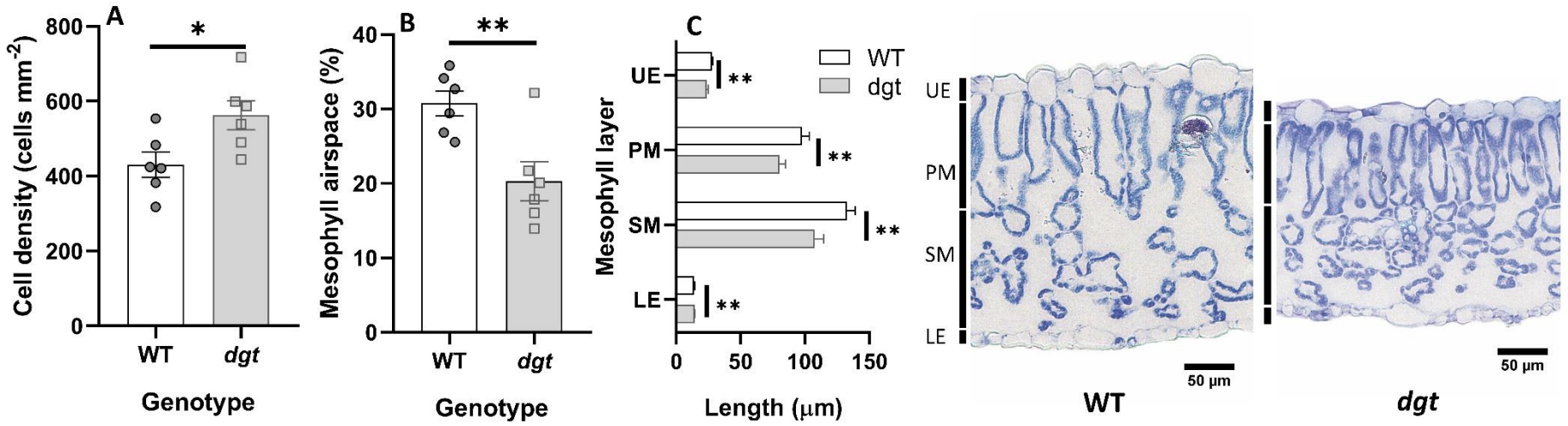

Fig. S3. (A) Mesophyll cell density, (B) mesophyll airspace, (C) thickness of upper epidermis (UE), palisade mesophyll (PM), spongy mesophyll (SM), and lower epidermis (LE) of WT and *dgt* mutants. Representative images of cross-sectional images of leaves are depicted in C. Data are mean ± SE (n = 6). Asterisks indicate significant change between genotypes according to Student's t test. ** = $P < 0.01$

CHAPTER 2

Impaired auxin signaling increases hydraulic safety and water deficit tolerance in tomato

Moab T. Andrade, Leonardo A. Oliveira, Talitha S. Pereira, Eduardo J. Haverroth, Genaina A. Souza, Fábio M. DaMatta, Agustín Zsögön, Amanda A. Cardoso, Samuel C. V. Martins

Introduction

The long-distance transport of water from roots to shoots is fundamental for plant function, and the disruption of this process to a large extent can lead to crown dieback (Cardoso *et al.*, 2020*a*; Brodribb *et al.*, 2021) or even whole-plant mortality (Brodribb & Cochard, 2009; Sevanto et al., 2014). In terrestrial environments, the possibility of plants facing eventual water restriction is inherent to some biomes and, as a consequence, the water transport system requires the xylem to be a robust structure that can support increasing tension while water is in a metastable state.

Hydraulic safety represents the xylem's ability to resist drought-induced cavitation, thus maintaining the water supply to attend to the plant demands which are essential for its function and survival. Xylem cavitation consists of the breakdown of the water column; as xylem water is in a metastable state, small perturbations induce the transition to the gaseous state, resulting in nucleation and expansion of small bubbles (Tyree and Sperry, 1989). This results in embolized vessels in the system, which considerably reduce the efficiency of water transport (Tyree, 2003; Zimmermann et al., 2004). Drought-induced cavitation is best explained by the air-seeding model, which consists of disturbances caused by air seeding of nano-bubbles into sap-filed conduits via pit membranes (Schenk *et al.*, 2015). The pit membrane is a functional intervessel connection, consisting of a small portion (c. 4.8 µm in diameter) of the primary cell wall composed mainly of c. 20 nm wide cellulose microfibril aggregates, where the secondary cell wall is not deposited, and the middle lamella is enzymatically degraded (Jansen *et al.*, 2009; Kaack *et al.*, 2019, 2021). The pit membranes are also involved in gas entry from embolized (gas-filled) vessels to sap-filled ones, playing a

crucial role in embolism resistance and embolism spread (Knipfer *et al.*, 2015; Avila *et al.*, 2022).

Xylem embolism resistance has been observed to be associated with structural parameters of the xylem conduits, such as conduit diameter (D_h) and density, pit membrane thickness and porosity, and pit border and chamber depth (Choat *et al.*, 2008; Jansen *et al.*, 2009; Lens *et al.*, 2011; Kaack *et al.*, 2019). In the case of freeze-induced cavitation, it is well accepted that there is a causal relationship between the reduction of the D_h and a higher embolism resistance, due to the reduced cross-section of the vessel reducing the number of microbubbles that could swell during thawing (Davis *et al.*, 1999; Pittermann and Sperry, 2006; Olson *et al.*, 2018). On the other hand, in drought-induced cavitation, there is no direct relationship with D_h, but the logical assumption is that small conduits have less vessel wall surface area, hence a tendency to have a smaller membrane area as well. Hacke et al. (2006) verified a strong relationship (r^2= 0.77) between increased embolism resistance (represented by the water potential at which 50% of the xylem conduits are embolized, Ψ_{50}) and reduced pit membrane area (A_p) in 29 angiosperm species from a wide phylogenetically range. However, these associations between embolism resistance and xylem structure are mostly inferred based on interspecific data from wood plants, and studies within species, especially herbs, are scarce. The ratio $(t/b)^3$ which relates the conduit wall thickness (t) and conduit breadth or lumen (b) is another parameter that is associated with higher embolism resistance (Hacke *et al.*, 2001; Cardoso *et al.*, 2018).

The recent development of a new non-destructive method to assess xylem embolism resistance in soft organs and plants (i.e. the optical vulnerability method) (Brodribb *et al.*, 2016) has allowed scientists to better understand drought-induced challenges to the water transport in herbaceous plants (Skelton *et al.*, 2017; Cardoso *et al.*, 2018; Johnson *et al.*, 2018; Lamarque *et al.*, 2020) These studies indicate that herbaceous species, including tomato, are relatively vulnerable to drought-induced embolism and thus likely susceptible to hydraulic failure and mortality during drought. Another interesting fact is the large intra-specific variability in the xylem resistance to embolism (Lamarque *et al.*, 2020), which raises the questions of what are the internal and external cues associated with this variation and whether we can manipulate these factors to produce cultivars that are more tolerant to drought.

The tomato mutant *dgt* has been recently described as presenting smaller D_h compared to its wild-type (Batista-Silva *et al.*, 2019; Andrade *et al.*, 2022), which provides an opportunity to assess whether changes in the xylem structure affect embolism resistance within this species. Associated with the reduction in D_h, *dgt* showed lower stomatal conductance and higher intrinsic water use efficiency (Andrade *et al.*, 2022). We hypothesize that the conduit diameter reduction in *dgt* will result in greater resistance to drought-induced embolism, which might provide greater water deficit tolerance. To test this, we characterized the structural changes in the xylem (i.e. Dh, $(t/b)^3$, pit aperture, and A_p) and assessed embolism resistance in leaves of *dgt* and wild-type plants. Finally, we exposed both genotypes to water deficit by withholding irrigation to assess whether potential changes in embolism resistance would result in greater tolerance to water deficit.

Materials and methods

Plant material

Plants of *dgt* and its WT (background Ailsa Craig) (Oh *et al.*, 2006) were cultivated from seeds in a greenhouse in Viçosa (20° 45' 37" S 42° 52' 04" W), Brazil. Seeds were cultivated in a commercial substrate (Tropstrato HT®), and the seedlings were transplanted into 5-L pots (one individual per pot) containing the same substrate soon after the appearance of the first true leaf. Plants utilized for the water deficit experiments were planted in similar size pots containing a 2:2:1 (v:v:v) mixture (clayey soil, sand, and commercial substrate) to increase the dehydration time and allow data collection. All the plants were cultivated until they were approximately two-month-old. Conditions in the greenhouse were *c.* 1,500 µmol m^{-2} s^{-1} of maximum photosynthetic photon flux density (PPFD), with a photoperiod of around 12 h. The temperature ranged from 25.2 to 31.9°C and relative humidity, from 46 to 64%. Plants were weekly fertilized (around 2 g per plant) using a commercial NPK formulation (10:10:10).

Xylem anatomy

For light microscopy analyses, midribs and terminal petioles were sampled from the apical leaflet of completely expanded leaves from different plants (n = 6) inserted in the middle third of shoots. Stem samples were also collected from the same region of each plant (n = 6). All samples were fixed in FAA for 48 h (Johansen, 1940) and

stored in 70% ethanol in water (v/v). Before anatomical analyses, samples were dehydrated in a graded ethanol series and embedding according to manufacturer's instructions (Leica Historesin embedding kit, Leica Microsystems, Heidelberg, Germany). Sections (5-μm-thin) were obtained with an automatic rotary microtome (Leica RM 2155, Leica Microsystems Inc., Deerfield, USA), transferred to glass slides, stained with toluidine blue (O'Brien *et al.*, 1964), and mounted in Permount® resin. Images were taken using a digital camera (Zeiss AxioCam HRc, Göttinger, Germany) mounted on a light microscope (AX70 TRF, Olympus Optical, Tokyo, Japan). Measurements were performed using Image-Pro Plus 4.5 (Media Cybernetics, Silver Spring, USA). The hydraulically weighted diameter of xylem conduits (D_h) was determined for stems, petioles, and midribs following Kolb and Sperry (1999). The xylem cell wall thickness (*t*) and lumen width (*b*), for the ratio $[(t/b)^3]$ (was measured in all conduits of the midrib, petiole, and stem; for each *b* the average of the maximum and minimum conduit diameters was used, and *t* was obtained by averaging four random measurements of cell wall thickness.

The pit membrane analysis was performed in samples (n = 4) collected from the median portion of the stem that was fixed in Karnovsky solution. Next, the cryofracture was performed by pre-soaking samples in glycerol (30 min), immersing them in liquid nitrogen, and then splitting with a blade. The samples were then dehydrated by immersion in ethyl series (30, 50, 70, 90, and 99%), dried in a critical point dryer instrument (Balzers CPD-030), placed on stub with double adhesive carbon conductive tape, and sputter-coating with gold in Quorum Q150R S coater. The vessel elements and pit membranes were observed in a scanning electron microscope (LEO 1430 VP, Carl Zeiss, Germany). From these samples, we measured the individual pit membrane area (A_{pm}, μm^2) and maximum diameter of pit membrande (D_{pm}; μm; minimum of 85 measurements per genotype). All measurements were made using ImageJ (National Institutes of Health, Bethesda, USA).

Pressure-volume curves and xylem resistance to embolism

Pressure-volume curves (Tyree & Hammel, 1972) were performed using completely expanded leaves (*n* = 8) that were cut under water and rehydrated overnight until Ψ_{leaf} was c. -0.1 MPa. On the next morning, leaves were allowed to slowly desiccate, while leaf weight and Ψ_{leaf} were regularly assessed until Ψ_{leaf} stopped falling due to cellular damage. In the end, leaves were scanned and had their leaf area

and dry weight measured. Leaf dry weights were utilized to calculate relative water content (RWC), which were next plotted against Ψ_{leaf}^{-1}. From each curve, we estimated the saturated water content (SWC), the water potential and the RWC at turgor loss point (Ψ_{TLP} and RWC_{TLP}), the osmotic potential at full turgor (Ψ_s), the global modulus of elasticity (ε), and the leaf capacitance at full turgor (C_{FT}) and turgor loss point (C_{TLP}) normalized by leaf area.

Leaf vulnerability to embolism was determined by the recently developed optical vulnerability method (Brodribb et al., 2016). Well-watered plants (n = 7) had their roots carefully washed to remove the soil and they were next transported to the laboratory while their roots were maintained under water. Intact leaves from each plant were placed on an electronic photo scanner (Epson perfection V800 Scanner; Epson America, Long Beach, USA) while still attached to the plants. The roots were removed from the water and plants were allowed to slowly dehydrate under laboratory conditions (28 ± 2.3°C and 48 ± 2.5% relative humidity). During plant dehydration, leaves were scanned every 4 min using a resolution of 4000 dpi, and the Ψ_{leaf} of neighboring expanded leaves was assessed every 1-2 h using a pressure chamber. Images were analyzed following the instructions of Brodribb et al. (2016) and the OpenSourceOV (https://www.opensourceov.org/). Finally, we plotted the percentage of the embolized area against Ψ_{leaf} to construct the vulnerability curves (mean ± SE). From each curve, we determined the Ψ_{leaf} at 12, 50, and 88% of the embolized area (Ψ_{12}, Ψ_{50}, and Ψ_{88}) and we calculated the slope (% MPa^{-1}) of the curve as Slope = (88 – 12)/ ($\Psi_{12} - \Psi_{88}$) (Domec & Gartner, 2001).

Water deficit experiments

Both genotypes dried down to their respective Ψ_{50}

At c. 45 days after planting, we imposed a water deficit stress by withholding the irrigation until the Ψ_{50} obtained in the OV curve (i.e., -1.14 MPa for the WT and -1.39 MPa for the *dgt*). The water potential was monitored every two days at c. 12:00 (solar time) by sampling leaves and measuring them with a Scholander pressure chamber (Model 1000, PMS Instruments, Albany, USA) until the mean (n = 6) Ψ_{leaf} of each genotype achieved their respective Ψ_{50}. After that, plants were irrigated and maintained under well-watered conditions to assess the plant recovery (for additional c. 4 days). Leaf gas exchange was measured every two days during irrigation suspension and

every day after rehydration using an infra-red gas analyzer (LI-6400XT, LI-COR, Lincoln, USA). Measurements were taken on fully expanded leaves in the middle third of the plant between 09:00 and 12:00 (solar time) when gas exchange was expected to be maximal. Conditions within the leaf cuvette were 1,000 µmol m^{-2} s^{-1} PPFD (10% of blue light), 400 µmol CO_2 mol^{-1} air, and vapor pressure deficit at approximately 1.0 kPa. After reaching the steady-state, net CO_2 assimilation rate (A_n), stomatal conductance to water vapor (g_s), and transpiration rate (E) were recorded. Whole-plant transpiration (E_g) was daily assessed through the gravimetrical method and further normalized utilizing data from pots without plants under the same conditions (n = 3). Finally, the soil moisture (θ_g) was daily estimated based on the saturated water content and dry weight of control pots and calculated as θ_g = (SW – DSW)/ (SSW – DSW), where SW is the daily measured pot weight, DSW is the dry soil weight, and SSW is the soil saturated weight. The whole plant hydraulic conductance (K_{plant}) was also assessed according to the evaporative flux method (Tsuda and Tyree, 2000) by evaluating the predawn and midday Ψ_{leaf} and the E_g, measuring the mass of the pots in the same time (6 h period) and then normalizing by plant leaf area, which was measured in LI-3100C area meter.

WT dried down to the dgt Ψ_{50}

To verify if the increased xylem embolism resistance of *dgt* had any physiological significance, we performed a second water deficit experiment using the WT. Plants were then exposed to a more severe water deficit level (c. -1.39 MPa, which corresponds to the *dgt* Ψ_{50}). Water potentials and leaf gas exchange were monitored as previously described. Additionally, at end of the experiment, the K_{leaf} was measured in the same leaves used to measure leaf gas exchange (n = 6) *via* the evaporative flux method (Sack *et al.*, 2002; Brodribb and Holbrook, 2006). Those experiments were performed from 08:00 to 16:00 (solar time) when leaves had their petioles cut under water, connected to a flowmeter (equipped with a pressure transducer 30Psi – Honeywell International), and placed under c. 1,000 µmol m^{-2} s^{-1} PPFD and fan-induced turbulent air to increase leaf transpiration. The pressure variation, the water temperature, and the leaf temperature were recorded with a high-resolution datalogger (Campbell Scientific, model: CR1000). The transpiration rate (E) was derived from the tension created within the flowmeter system driven by leaf through a known resistance and logged following maximum stability (after c. 30 min). Leaves were then removed

from the system, bagged for c. 15 min (to allow leaf equilibration), and had their water potential (Ψ_{leaf}) measured with a Scholander pressure chamber (Model 1000, PMS Instruments, Albany, USA). After that, leaves were scanned and their area was measured using ImageJ (National Institutes of Health, Bethesda, USA). Finally, *E* was normalized by leaf area and K_{leaf} was calculated as $K_{leaf} = -E/\Psi_{leaf}$.

Statistical analysis

Morphological, anatomical, and physiological traits between the two genotypes were compared by unpaired Student's t-tests ($\alpha < 0.05$). For both water deficit experiments, we performed ordinary one-way ANOVA and Tukey's multiple comparisons tests ($\alpha < 0.05$) for some traits. Statistical analyses and the graphs were generated using GraphPad Prism 8.0 (GraphPad Software, San Diego, USA).

Results

The xylem vessels of *dgt* mutants were consistently smaller than the WT, with a reduced cross-section hydraulic weighted vessel diameter (D_h) of the stem (-24%), petiole (-43%), and midrib (-34%) (Fig. 1A-B and Fig. S1). The *dgt* mutants showed a similar number of xylem conduits for stems and midrib relative to WT, however, it was lower for the petiole (Fig. 1C). The *dgt* mutants showed a ratio t/b^3 consistently greater than WT in all tissues analyzed.

Electron microscopy analysis reaffirmed the smaller caliber of the xylem vessels of the *dgt* mutant compared to the WT (Fig. 2A and D). However, the pit membrane area and maximum diameter were similar between genotypes (Fig. 2G-H).

Among pressure-volume curve parameters, the RWC_{TLP} of *dgt* was 5% lower than WT (Table 1) whereas no significant differences were found for the other parameters (Ψ_{TLP}, Ψs, and the leaf capacitances) (Table 1).

The embolism optical vulnerability was contrasting between genotypes (Fig. 3). Briefly, the cavitation events started with a lower dehydration level in WT than *dgt*, despite Ψ_{12} did not differ significantly (Table 1). Indeed, only Ψ_{50} values were different with the *dgt* mutant presenting a Ψ_{50} 0.25 MPa more negative than the WT. As there was no difference in Ψ_{TLP}, the *dgt* had a hydraulic safety margin (HSM) c. 64% greater compared with WT (Fig. 3A). Also, the curve slope was different between genotypes,

with *dgt* demanding a larger dehydration range to embolize all leaf veins, especially the minor veins (Fig. 3B-C).

To achieve their respective Ψ_{50}, the *dgt* mutant endured twice as much irrigation suspension time (12 days) compared to WT (6 days; Fig. 4A-B). At this time, the plants had extracted more than 60% of the soil moisture (Fig. 4C), and leaf gas exchange parameters indicated severe inhibition of photosynthetic activity (Fig. 4D-E). In turn, the recovery after rehydration of the *dgt* mutant was faster than the WT. Whereas *dgt* plants took two days to recover net photosynthetic rates and stomatal conductance to control levels, WT required four days to achieve the same (Fig. 4D-E). In addition, when WT plants were submitted to *dgt* Ψ_{50}, i.e. -1.39 MPa, the time to reach the water deficiency was lower (8 days) than *dgt* (Fig. 5A and C). Noteworthy, although after one day of rehydration (9th day) the tomato plants visually recovered turgor (Fig. 5B), their leaf gas exchange parameters did not recover to the control levels even after sixteen days of evaluation (Fig. 5D-E).

Discussion

The *dgt* mutation alters the xylem anatomy and embolism resistance

The vulnerability curves showed Ψ_{50} values significantly more negative for the *dgt* mutant, consistent with the reported trend of higher embolism resistance in species with reduced vessel diameter and higher $(t/b)^3$. In this study, we confirmed the reductions in conduit diameter in leaves of the *dgt* mutant as previously observed (Batista-Silva *et al.*, 2019; Andrade *et al.*, 2022). This result suggests an association of *DGT* function with the regulation of cell expansion during the development of leaf xylem conduits. Given the key role of auxin in xylem development, the impaired auxin perception due to *dgt* mutation might have affected cell wall acidification and impaired cell growth. Indeed, it was previously reported the inability of tomato *dgt* hypocotyls to activate membrane H^+-ATPase (Coenen *et al.*, 2002, 2003).

Whereas it is well accepted that there is a causal relationship between the reduction of the conduit diameter and higher embolism resistance in the case of freeze-induced embolism, the mechanistic explanation of the association between reduced conduit diameter and drought-induced embolism resistance remains unclear. It has been suggested that small conduits have less vessel wall surface area, hence a tendency to have smaller pit membrane area, and thus higher pit membrane stiffness

and resistance to embolism (Hacke *et al.*, 2006). However, it is unclear whether reducing the vessel cross-section “per se” without changes in the properties and frequency of the pit membrane could contribute to increased xylem safety.

We speculate that reducing the cross-section of the conduits may favor improved resistance to cavitation. Since physical interactions between solid surfaces and water are stronger than water-water interactions, we assume that increased interaction with the vessel wall may result in increases in tensile strength. With a reduction in conduit diameter, there is a direct increase in the proportion of water molecules committed to hydrogen bonds at the circumference of the water-conduit interface; thus, the proportional amount of water interacting with the cell wall is greater. Additionally, two pieces of evidence seem to support that water-cell wall interactions in the xylem may play a role in embolism resistance. In particular, the lignin monomeric composition of xylem cell wall conduits affects the embolism resistance (Lima *et al.*, 2018; Pereira *et al.*, 2018). Another possibility is the existence of ion-mediated interactions among water-ion-cell wall, which affect the xylem hydraulic conductivity (Zwieniecki *et al.*, 2001; Nardini *et al.*, 2011).

We also observed an increased $(t/b)^3$ in leaves of the *dgt* mutant (Fig. 1B and C) and, similarly to a reduced conduit diameter, a higher $(t/b)^3$ is typically observed in association with higher drought-induced resistance to embolism in woody and herbaceous plants (Hacke *et al.*, 2001; Cardoso *et al.*, 2018). There is still no mechanistic explanation of how this characteristic relates to embolism propagation, but changes have been observed within some species leading to the belief that higher $(t/b)^3$ may reflect a xylem adaptation to resist more negative pressures (Zhang *et al.*, 2016; Cardoso *et al.*, 2018; Avila *et al.*, 2022). For now, the reason why $(t/b)^3$ is associated with embolism resistance is generally attributed to changes in the conduit mechanical resistance to implosion (due to increases in cell wall thickness) which is accompanied by thicker and more resistant pit membranes (Hacke *et al.*, 2001; Lens *et al.*, 2011).

Interestingly, the *dgt* mutant showed higher $(t/b)^3$ than WT in all organs analyzed, but this was not associated with cell wall reinforcement. In fact, there was a significant 23% reduction in cell wall thickness (*t*) of *dgt* (1.81±0.04 µm) compared to WT (2.34±0.15 µm). This reduction in *t* was compensated by an even greater reduction in xylem lumen breadth (*b*) resulting in higher $(t/b)^3$. Within the same botanical group, e.g., angiosperms, species with higher $(t/b)^3$ tend to have better cavitation resistance,

showing more negative Ψ_{50} (Hacke *et al.*, 2001). As *dgt* showed no cell wall reinforcement, this suggests that changes in vessel embolism resistance may be due to a different factor. Noteworthy, we wonder to what extent this reduction in *t* in *dgt* is associated with its inability to activate membrane H^+-ATPase, and, consequently, a decreased capacity for apoplast acidification.

As the air seeding hypothesis suggests, cavitation occurs when nanobubbles are drawn across the pit membranes from an embolized conduit to a sap-filled conduit, impairing water transport (Lens *et al.*, 2011; Brodersen *et al.*, 2014; Jacobsen *et al.*, 2019). The presence of a malformed pit membrane (i.e. rare pit membrane hypothesis) may favor the entry of air into xylem conduits; thus, a higher pit membrane area increases the chances of cavitation occurrence (Hacke *et al.*, 2006; Christman *et al.*, 2009, 2012). Interestingly, the reduction in vessel diameter in *dgt* mutant was not accompanied by changes in pit area compared to WT (Fig. 2G). To maintain the same ratio in smaller conduits one would expect a reduction in pit size, however, the pit pore aperture diameter also did not differ significantly between *dgt* and WT (Fig. 2H). In any case, the membrane area alone does not fully explain variations in Ψ_{50}. The “pit area hypothesis” has been supported by more evidence, but the presence of vestured pit, pit membrane thickness, membrane pore size, as well as pore constrictions also contribute to Ψ_{50} (Jansen *et al.*, 2009; Lens *et al.*, 2011; Kaack *et al.*, 2019, 2021). Thus, further work evaluating these complex characteristics would be necessary to understand the origin of the increased embolism resistance of *dgt*. These analyses are very complex and subject to sample preparation artifacts, requiring great technical expertise, perfusion with colloidal gold, and high-resolution transmission electron microscopy (TEM) for a three-dimensional view of the pit membranes (Zhang *et al.*, 2020). However, such features may correlate with simple analytical traits (e.g. cell wall thickness, membrane thickness, pit area, $(t/b)^3$), but a large number of studies are required to ascertain the existence of such correlations.

The *dgt* mutation confers higher water deficit tolerance

The difference of 0.25 MPa in Ψ_{50} of the *dgt* mutant may not seem relevant when considering the xylem tension developed in severe drought events. However, this change may be decisive in maintaining water transport and recovery after stress relief. In addition, after stomatal closure, the minimum rates of water loss through the epidermal cuticle determine how long plants will survive if drought conditions continue

(Körner, 2019; McDowell *et al.*, 2019). The reduction of Ψ_{50} in *dgt* resulted in greater HSM, i.e., the difference between water potential at stomatal closure (inferred by Ψ_{TLP}) and Ψ_{50}.

In the water deficit experiments, the *dgt* spent twice as much time compared to WT to reach the stress level of their respective Ψ_{50}. This result was expected due to the significant difference in leaf area between genotypes, as the larger transpiratory area of WT contributes to rapid water loss and reduced water status. Regarding the dynamics of post-stress recovery, it is still poorly understood in herbaceous plants, as studies generally focus on growth recovery in woody plants (Ruehr *et al.*, 2019). Indeed, the *dgt* mutant had a faster leaf gas exchange recovery after rehydration than WT plants. Considering that both genotypes were subjected to the same level of stress, i.e. the loss of 50% of the hydraulic conductivity, it is curious how quickly was the *dgt* recovery in contrast to WT. We suggest that xylem vessels with reduced diameter might be more prone to refilling by capillary forces, root pressure, or even less need for non-structural carbohydrates (if considering the active refilling process). After rehydration, *dgt* and WT plants showed a K_{plant} reduction of 39% and 47%, respectively, when compared with well-watered plants (Fig. S2). This confirms that our experiment was effective in causing c. 50% of embolism and that *dgt* showed a moderate recovery of plant hydraulic conductivity whereas WT did not show any recovery at all. Such impairment in K_{plant} partially explains why Ψ_{leaf} did not recover to control levels even after 3 days following rehydration in WT plants (Fig. 4B).

Despite differences in the speed of stress establishment and recovery, both genotypes showed similar recovery in net CO_2 assimilation and stomatal conductance to the control levels. However, when WT was dehydrated to Ψ_{leaf} corresponding to *dgt´*s Ψ_{50}, we again observed faster dehydration, but this time there was no recovery of Ψ_{leaf} or gas exchange. The severe stress caused a marked wilting on the distal part of some leaves that was reversed only on the second day after rehydration (personal observation). Brodribb *et al.* (2021) also observed that rapid dehydration causes tissue collapse in distal regions of leaves in tomato, linking hydraulic failure with severe physiological damage. We assume that there was no such damage in our plants because cell turgor recovered, i.e. total hydraulic failure did not happen. It seems that the difference in dehydration speed may be decisive for the plant to respond to the stress by changing its metabolism and gene expression to mitigate the deleterious

stress effects. After two days of rehydration, the stressed plants were visually similar to the control; however, as leaf gas exchange did not recover, this indicates that the additional tension of 0.25 MPa did impact the ability to recover photosynthetic activity. We verified an 88% reduction of K_{leaf} in stressed plants (Fig. S2C), consistent with the Ψ_{88} value found on the vulnerability curve (c. -1.45 MPa), and this reduction of water transport capacity in the leaf may be related to the inhibition of gas exchange.

Interestingly, it seems that the photosynthetic recovery of tomato leaves depends on the degree of embolism and that photosynthesis rates are limited by the remaining water transport capacity. These observations indicate the possibility that the protoplast could withstand further dehydration and recover, provided that the water supply remained operational. In *Persea americana*, xylem resistance to embolism determines leaf mortality in drought-stressed plants, in a well-coordinated pattern between leaf necrotic area and embolism percentage (Cardoso *et al.*, 2020*a*). Here, we did not observe leaf necrosis, which indicates that the embolism did not directly result in tissue damage. This observation is supported by the well-established sequence of events during dehydration, which shows that reductions in rehydration capacity and chlorophyll fluorescence values occur at water potentials more negative than Ψ_{50} (Trueba *et al.*, 2019; Oliveira *et al.*, 2022).

Conclusion

The auxin perception mutation results in xylem vessels with reduced diameter and higher $(t/b)^3$, but without major modifications in the pit membranes and cell wall reinforcement, which makes *dgt* an excellent model to verify the isolated effects of changes in these parameters on cavitation vulnerability. The changes in *dgt* xylem architecture resulted in a 0.25 MPa more negative Ψ_{50} and a 64% higher HSM, indicating an advantage over WT plants in a water-limited condition. This advantage was confirmed as *dgt* was exposed to a more negative Ψ_{leaf} than WT plants and still presented a faster recovery of leaf gas exchange. On the other hand, when WT plants were exposed to *dgt*'s Ψ_{50}, they did not show photosynthetic recovery, confirming the result of the vulnerability curve and the increased hydraulic safety of the *dgt* mutant.

References

Andrade MT, Oliveira LA, Pereira TS, Cardoso AA, Batista-Silva W, DaMatta FM, Zsögön A, Martins SC V. 2022. Impaired auxin signaling increases vein and stomatal density but reduces hydraulic efficiency and ultimately net photosynthesis (T Lawson, Ed.). Journal of Experimental Botany, 1–5.

Avila RT, Guan X, Kane CN, Cardoso AA, Batz TA, DaMatta FM, Jansen S, McAdam SAM. 2022. Xylem embolism spread is largely prevented by interconduit pit membranes until the majority of conduits are gas-filled. Plant, Cell & Environment **45**, 1204–1215.

Batista-Silva W, Medeiros DB, Rodrigues-Salvador A, *et al.* 2019. Modulation of auxin signalling through DIAGETROPICA and ENTIRE differentially affects tomato plant growth via changes in photosynthetic and mitochondrial metabolism. Plant Cell and Environment **42**, 448–465.

Brodersen C, Jansen S, Choat B, Rico C, Pittermann J. 2014. Cavitation resistance in seedless vascular plants: The structure and function of interconduit pit membranes. Plant Physiology **165**, 895–904.

Brodribb TJ, Brodersen CR, Carriqui M, Tonet V, Rodriguez Dominguez C, McAdam S. 2021. Linking xylem network failure with leaf tissue death. New Phytologist **232**, 68–79.

Brodribb TJ, Cochard H. 2009. Hydraulic failure defines the recovery and point of death in water-stressed conifers. Plant Physiology **149**, 575–584.

Brodribb TJ, Holbrook NM. 2006. Declining hydraulic efficiency as transpiring leaves desiccate: Two types of response. Plant, Cell and Environment **29**, 2205–2215.

Brodribb TJ, Skelton RP, Mcadam SAM, Bienaimé D, Lucani CJ, Marmottant P. 2016. Visual quantification of embolism reveals leaf vulnerability to hydraulic failure. New Phytologist **209**, 1403–1409.

Cardoso AA, Batz TA, McAdam SAM. 2020. Xylem embolism resistance determines leaf mortality during drought in persea americana. Plant Physiology **182**, 547–554.

Cardoso AA, Brodribb TJ, Lucani CJ, DaMatta FM, McAdam SAM. 2018. Coordinated plasticity maintains hydraulic safety in sunflower leaves. Plant Cell and Environment **41**, 2567–2576.

Choat B, Cobb AR, Jansen S. 2008. Structure and function of bordered pits- new discoveries and impacts on whole-plant hydraulic function. New Phytologist **177**, 608–626.

Christman MA, Sperry JS, Adler FR. 2009. Testing the 'rare pit' hypothesis for xylem cavitation resistance in three species of Acer. New Phytologist **182**, 664–674.

Christman MA, Sperry JS, Smith DD. 2012. Rare pits, large vessels and extreme vulnerability to cavitation in a ring-porous tree species. New Phytologist **193**, 713–720.

Coenen C, Bierfreund N, Lüthen H, Neuhaus G. 2002. Developmental regulation of H+-ATPase-dependent auxin responses in the diageotropica mutant of tomato (*Lycopersicon esculentum*). Physiologia Plantarum **114**, 461–471.

Coenen C, Christian M, Lüthen H, Lomax TL. 2003. Cytokinin inhibits a subset of diageotropica-dependent primary auxin responses in tomato. Plant Physiology **131**, 1692–1704.

Davis SD, Sperry JS, Hacke UG. 1999. The relationship between xylem conduit diameter and cavitation caused by freezing. American Journal of Botany **86**, 1367–1372.

Hacke UG, Sperry JS, Pockman WT, Davis SD, McCulloh KA. 2001. Trends in wood density and structure are linked to prevention of xylem implosion by negative pressure. Oecologia **126**, 457–461.

Hacke UG, Sperry JS, Wheeler JK, Castro L. 2006. Scaling of angiosperm xylem structure with safety and efficiency. Tree Physiology **26**, 689–701.

Jacobsen AL, Brandon Pratt R, Venturas MD, Hacke UG. 2019. Large volume vessels are vulnerable to water-stress-induced embolism in stems of poplar. IAWA Journal **40**, 4–22.

Jansen S, Choat B, Pletsers A. 2009. Morphological variation of intervessel pit membranes and implications to xylem function in angiosperms. American Journal of Botany **96**, 409–419.

Johansen DA. 1940. *Plant microtechnique*. London: McGraw-Hill Book Company, Inc.

Johnson KM, Jordan GJ, Brodribb TJ. 2018. Wheat leaves embolized by water stress do not recover function upon rewatering. Plant Cell and Environment **41**, 2704–2714.

Kaack L, Altaner CM, Carmesin C, *et al.* 2019. Function and three-dimensional structure of intervessel pit membranes in angiosperms: A review. IAWA Journal **40**, 673–702.

Kaack L, Weber M, Isasa E, *et al.* 2021. Pore constrictions in intervessel pit membranes provide a mechanistic explanation for xylem embolism resistance in angiosperms. New Phytologist **230**, 1829–1843.

Knipfer T, Brodersen CR, Zedan A, Kluepfel DA, McElrone AJ. 2015. Patterns of drought-induced embolism formation and spread in living walnut saplings visualized using X-ray microtomography. Tree Physiology **35**, 744–755.

Kolb KJ, Sperry JS. 1999. Differences in drought adaptation between subspecies of sagebrush (Artemisia tridentata). Ecology **80**, 2373–2384.

Körner C. 2019. No need for pipes when the well is dry—a comment on hydraulic failure in trees. Tree Physiology **39**, 695–700.

Lamarque LJ, Delzon S, Toups H, *et al.* 2020. Over-accumulation of abscisic acid in transgenic tomato plants increases the risk of hydraulic failure. Plant Cell and Environment **43**, 548–562.

Lens F, Sperry JS, Christman MA, Choat B, Rabaey D, Jansen S. 2011. Testing hypotheses that link wood anatomy to cavitation resistance and hydraulic conductivity in the genus Acer. New Phytologist **190**, 709–723.

Lima TRA, Carvalho ECD, Martins FR, *et al.* 2018. Lignin composition is related to xylem embolism resistance and leaf life span in trees in a tropical semiarid climate. New Phytologist **219**, 1252–1262.

McDowell NG, Brodribb TJ, Nardini A. 2019. Hydraulics in the 21st century. New Phytologist **224**, 537–542.

Nardini A, Salleo S, Jansen S. 2011. More than just a vulnerable pipeline: Xylem physiology in the light of ion-mediated regulation of plant water transport. Journal of Experimental Botany **62**, 4701–4718.

O'Brien TP, Feder N, McCully ME. 1964. Polyehromatic Staining of Plant Cell Walls by Toluidine Blue O. Protoplasma **59**, 1–8.

Oh KC, Ivanchenko MG, White TJ, Lomax TL. 2006. The *diageotropica* gene of tomato encodes a cyclophilin: A novel player in auxin signaling. Planta **224**, 133–144.

Oliveira LA, Cardoso AA, Andrade MT, Pereira TS, Araújo WL, Santos GA, Damatta FM, Martins SC V. 2022. Exploring leaf hydraulic traits to predict drought tolerance of Eucalyptus clones. Tree Physiology.

Olson ME, Soriano D, Rosell JA, *et al.* 2018. Plant height and hydraulic vulnerability to drought and cold. Proceedings of the National Academy of Sciences of the United States of America **115**, 7551–7556.

Pereira L, Domingues-Junior AP, Jansen S, Choat B, Mazzafera P. 2018. Is embolism resistance in plant xylem associated with quantity and characteristics of lignin? Trees - Structure and Function **32**, 349–358.

Pittermann J, Sperry JS. 2006. Analysis of freeze-thaw embolism in conifers. The interaction between cavitation pressure and tracheid size. Plant Physiology **140**, 374–382.

Ruehr NK, Grote R, Mayr S, Arneth A. 2019. Beyond the extreme: Recovery of carbon and water relations in woody plants following heat and drought stress. Tree Physiology **39**, 1285–1299.

Sack L, Melcher PJ, Zwieniecki MA, Holbrook NM. 2002. The hydraulic conductance of the angiosperm leaf lamina: a comparison of three measurement methods. Journal of Experimental Botany **53**, 2177–2184.

Schenk HJ, Steppe K, Jansen S. 2015. Nanobubbles: A new paradigm for air-seeding in xylem. Trends in Plant Science **20**, 199–205.

Sevanto S, Mcdowell NG, Dickman LT, Pangle R, Pockman WT. 2014. How do trees die? A test of the hydraulic failure and carbon starvation hypotheses. Plant, Cell and Environment **37**, 153–161.

Skelton RP, Brodribb TJ, Choat B. 2017. Casting light on xylem vulnerability in an herbaceous species reveals a lack of segmentation. New Phytologist **214**, 561–569.

Trueba S, Pan R, Scoffoni C, John GP, Davis SD, Sack L. 2019. Thresholds for leaf damage due to dehydration: declines of hydraulic function, stomatal conductance and cellular integrity precede those for photochemistry. New Phytologist **223**, 134–149.

Tsuda M, Tyree MT. 2000. Plant hydraulic conductance measured by the high pressure flow meter in crop plants. Journal of Experimental Botany **51**, 823–828.

Tyree MT. 2003. The ascent of water. Nature **423**, 923.

Tyree MT, Sperry JS. 1989. Vulnerability of xylem to cavitation and embolism. Annual Review of Plant Biology **40**, 19–38.

Zhang Y, Carmesin C, Kaack L, *et al.* 2020. High porosity with tiny pore constrictions and unbending pathways characterize the 3D structure of intervessel pit membranes in angiosperm xylem. Plant Cell and Environment **43**, 116–130.

Zhang YJ, Rockwell FE, Graham AC, Alexander T, Michele Holbrook N. 2016. Reversible leaf xylem collapse: A potential 'circuit breaker' against cavitation. Plant Physiology **172**, 2261–2274.

Zimmermann U, Schneider H, Wegner LH, Haase A. 2004. Water ascent in tall trees: Does evolution of land plants rely on a highly metastable state? New Phytologist **162**, 575–615.

Zwieniecki MA, Melcher PJ, Holbrook NM. 2001. Hydrogel control of xylem hydraulic resistance in plants. Science **291**, 1059–1062.

Tables and Figures

Table 2. Leaf turgor loss point (Ψ_{TLP}), osmotic potential at full turgor (Ψs), relative water content at turgor loss point (RWC_{TLP}), global modulus of elasticity (ε), capacitance at full turgor (C_{FT}), capacitance at turgor loss point (C_{TLP}), and water potential at 12, 50 and 88% cumulative embolism (Ψ_{12}, Ψ_{50} and Ψ_{88}, respectively) for two genotypes of tomato plants, i.e. WT and the *dgt*:

Traits	WT	*dgt*
Ψ_{TLP} (MPa)	-0.81 ± 0.04	-0.88 ± 0.02^{ns}
Ψs (MPa)	-0.70 ± 0.04	-0.76 ± 0.02^{ns}
RWC_{TLP} (%)	90.11 ± 0.88	86.25 ± 0.97**
ε (MPa)	7.10 ± 0.84	6.86 ± 0.39^{ns}
C_{FT} (mol m^{-2} MPa^{-1})	1.17 ± 0.05	1.03 ± 0.7^{ns}
C_{TLP} (mol m^{-2} MPa^{-1})	3.10 ± 0.25	3.34 ± 0.53 ^{ns}
Ψ_{12} (MPa)	-0.90 ± 0.11	-1.07 ± 0.09^{ns}
Ψ_{50} (MPa)	-1.14 ± 0.08	-1.39 ± 0.06*
Ψ_{88} (MPa)	-1.45 ± 0.12	-1.71 ± 0.10^{ns}

Data are means ± SE (n = 6). Asterisks indicate significant genotypic differences according to Student's *t* test (^{ns} = not significant, * = $P < 0.05$, ** = $P < 0.01$)

Fig. 1. (A) Representative images of 50-day-old plants of tomato from the two genotypes, i.e. WT and *dgt* mutant. Representative cross-sectional images of petioles of WT (above) and *dgt* (below) mutant plants; (B) hydraulically weighted diameter of xylem conduits, (C) xylem conduits number, and (D) $(t/b)^3$ ratio in stem, petiole, and midrib. Bars are means ± SE (n=6). Symbols associated with bars are individual points. Asterisks indicate significant changes between genotypes according to Student's t test. ns = not significant. ** = $P < 0.01$.

Fig. 2. Representative micrography of xylem vessel, pit pore, and pit membrane of plants of tomato from two genotypes, i.e. WT (A-C) and *dgt* (D-F); (G) pit membrane area in relation to vessel wall area, and (H) pit pore aperture maximum diameter. Bars are means ± SE (n=4). Symbols associated with bars are individual points. Asterisks indicate significant change between genotypes according to Student's t test. ns = not significant.

Fig. 3. (A) Cumulative embolized xylem area (%) in leaves of WT and *dgt* mutants subjected to bench drying. The dashed vertical line in (A) indicates the mean leaf water potential at the turgor loss point for leaf (Ψ_{TLP}) and the dotted horizontal lines indicate the threshold of 12, 50, and 88% cumulative embolism. The inward box shows differences in leaf hydraulic safety margin (HSM = $\Psi_{50} - \Psi_{TLP}$). Data are mean (solid lines) ± SE (shaded area) (n = 7). Representative images depicting the sequence of embolism events observed in leaves of WT (B) and *dgt* mutants (C). Embolism events are marked by different colors corresponding to the Ψ_{leaf} at which embolisms occurred.

Fig. 4. (A) Representative image of tomato plants from control and water deficit treatments at their respective Ψ_{50} level, at 6 days for WT (-114 MPa) and 12 days for *dgt* (-1.39 MPa); (B) time course of predawn leaf water potential (Ψ_{leaf}) down to the Ψ_{50} level, (C) gravimetric estimation of soil moisture (D) net CO_2 assimilation rate and (B) stomatal conductance to water vapor during the experiment. Data are means ± SE (n = 6). Asterisks indicate significant genotypic differences according to Student's t test. ns = not significant. * = $P < 0.05$. ** = $P < 0.01$.

Fig. 5. (A) WT plants under *dgt* Ψ_{50} water deficit level (-1.39 MPa) and one day after rehydration (B); (C) time course of midday leaf water potential (Ψ_{leaf}) down to the *dgt* Ψ_{50} level; net CO_2 assimilation rate and (B) stomatal conductance to water vapor during experiment. Data are means ± SE (n = 6). Asterisks indicate significant genotypic differences according to Student's t test (* = P < 0.05, * = P < 0.05, ** = P < 0.01.

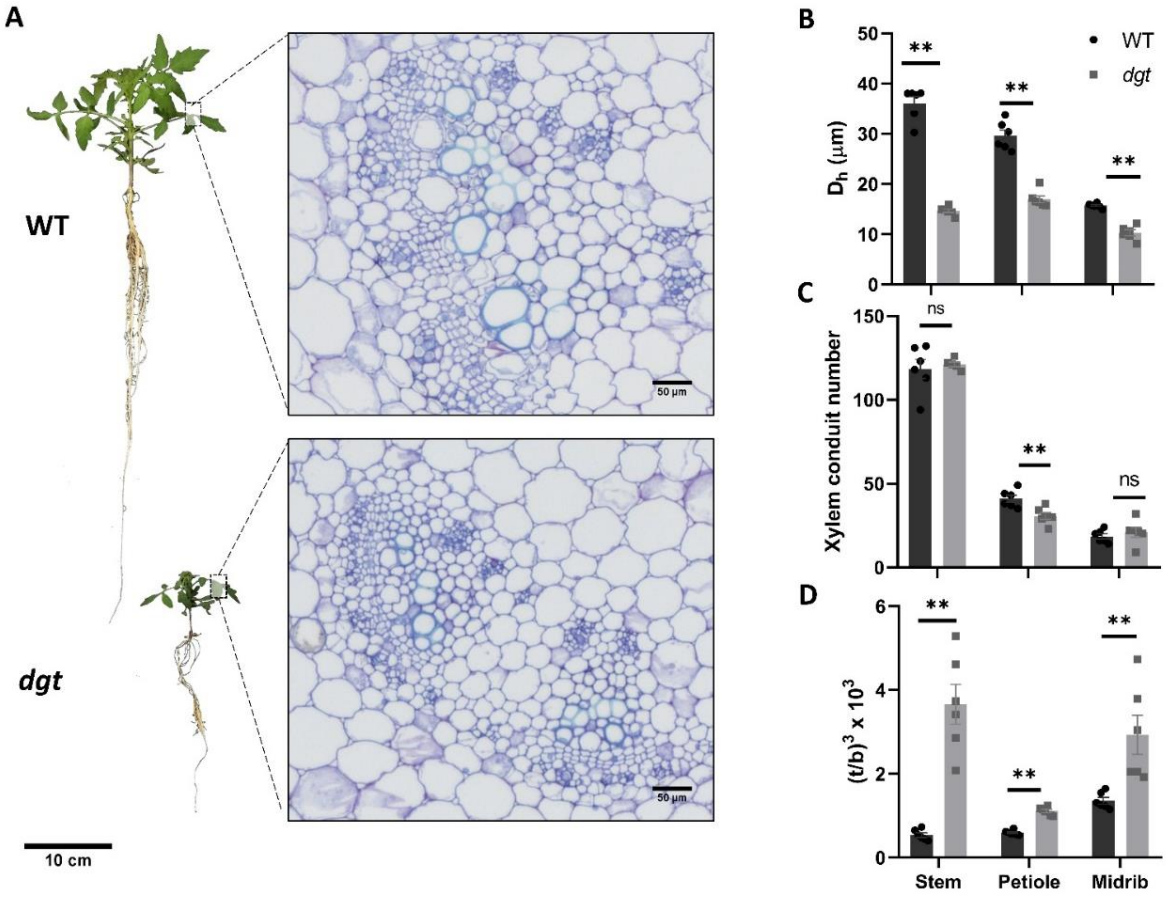

Figure 1.

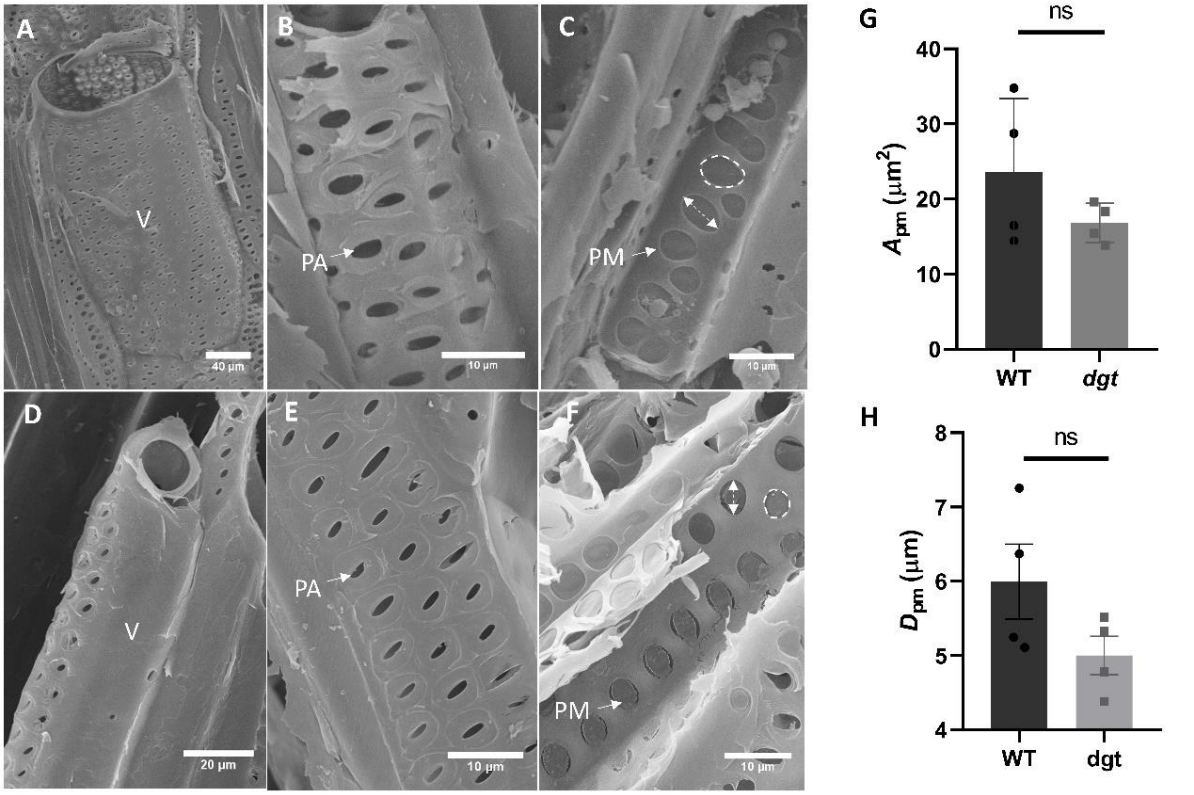

Figure 2.

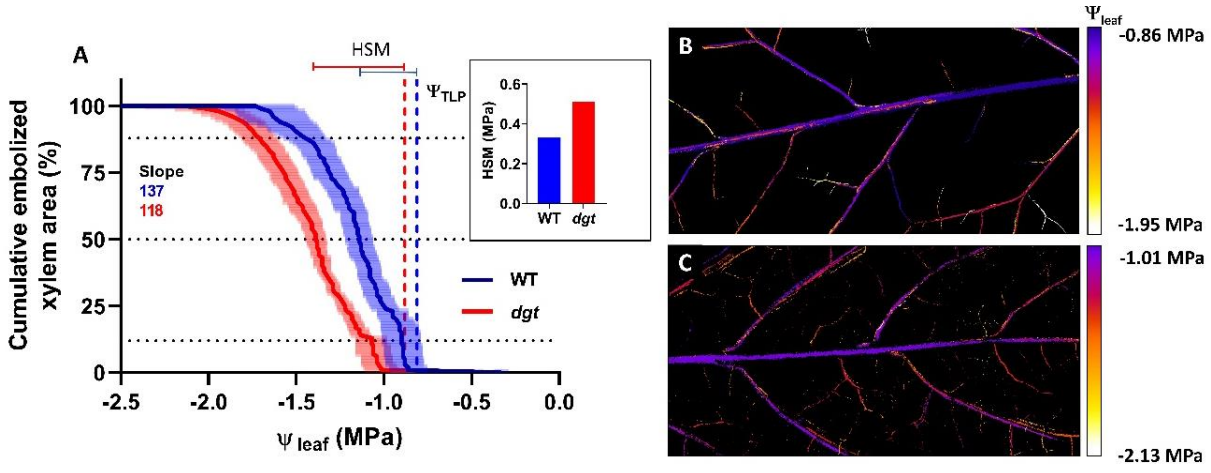

Figure 3.

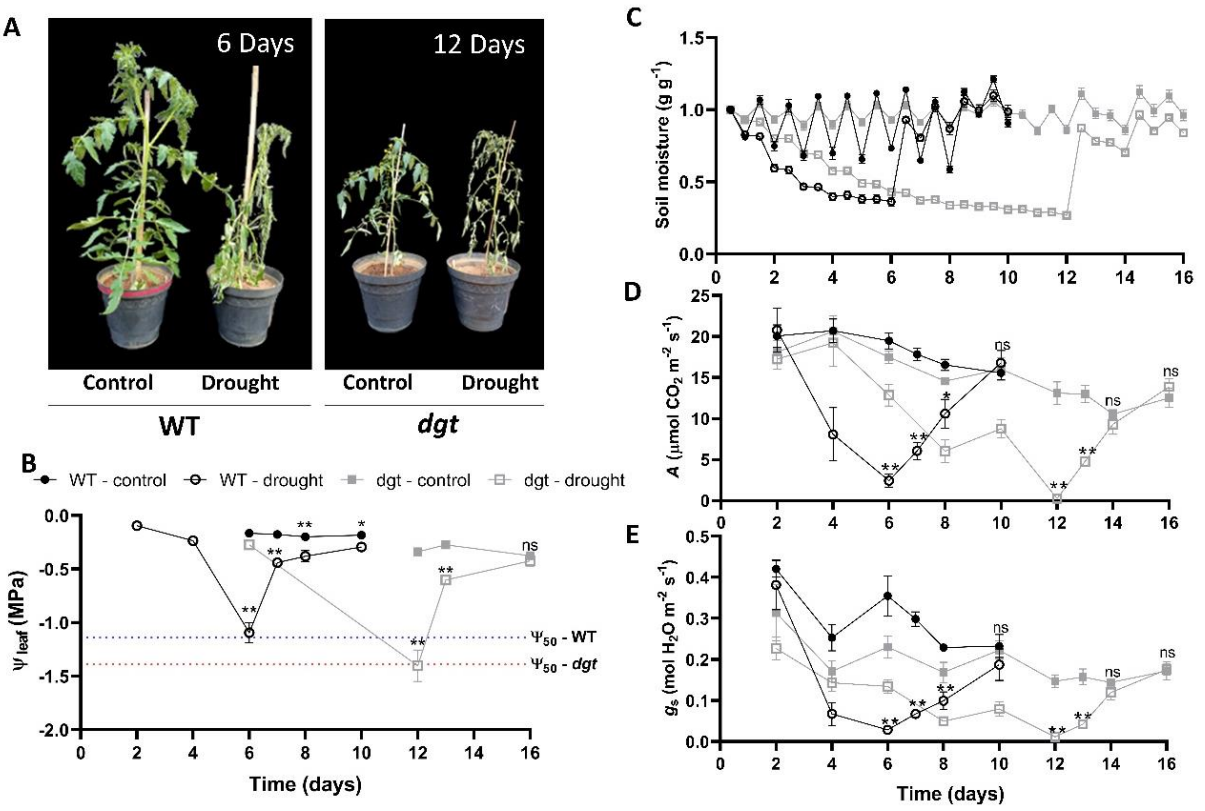
A
6 Days
12 Days
Control
Drought
Control
Drought
WT
dgt
B
WT - control
WT - drought
dgt - control
dgt - drought
Ψ leaf (MPa)
Ψ50 - WT
Ψ50 - dgt
Time (days)
C
Soil moisture (g g-1)
D
A (µmol CO2 m-2 s-1)
E
gs (mol H2O m-2 s-1)
Time (days)

Figure 4.

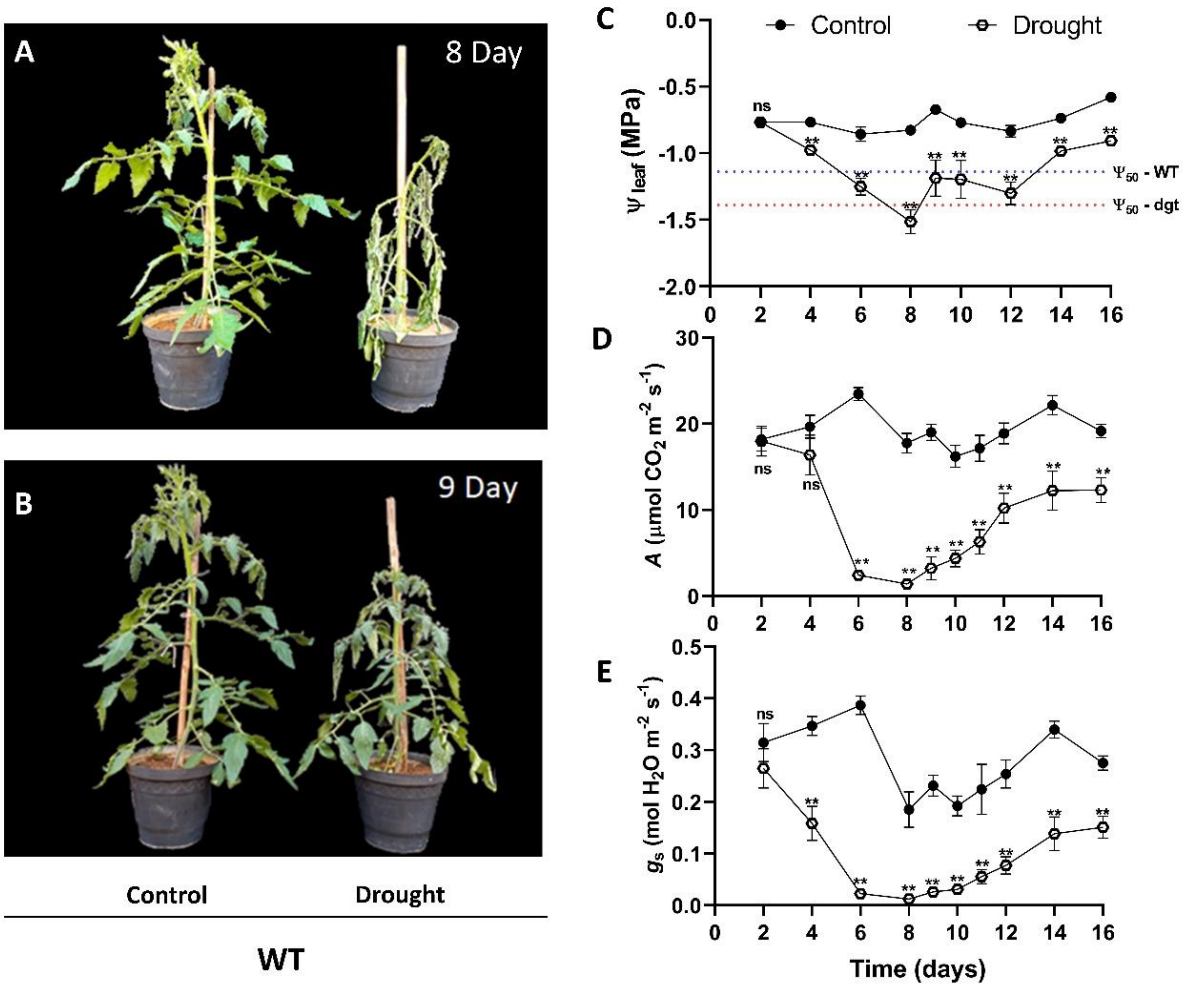

Figure 5.

Supplementary material

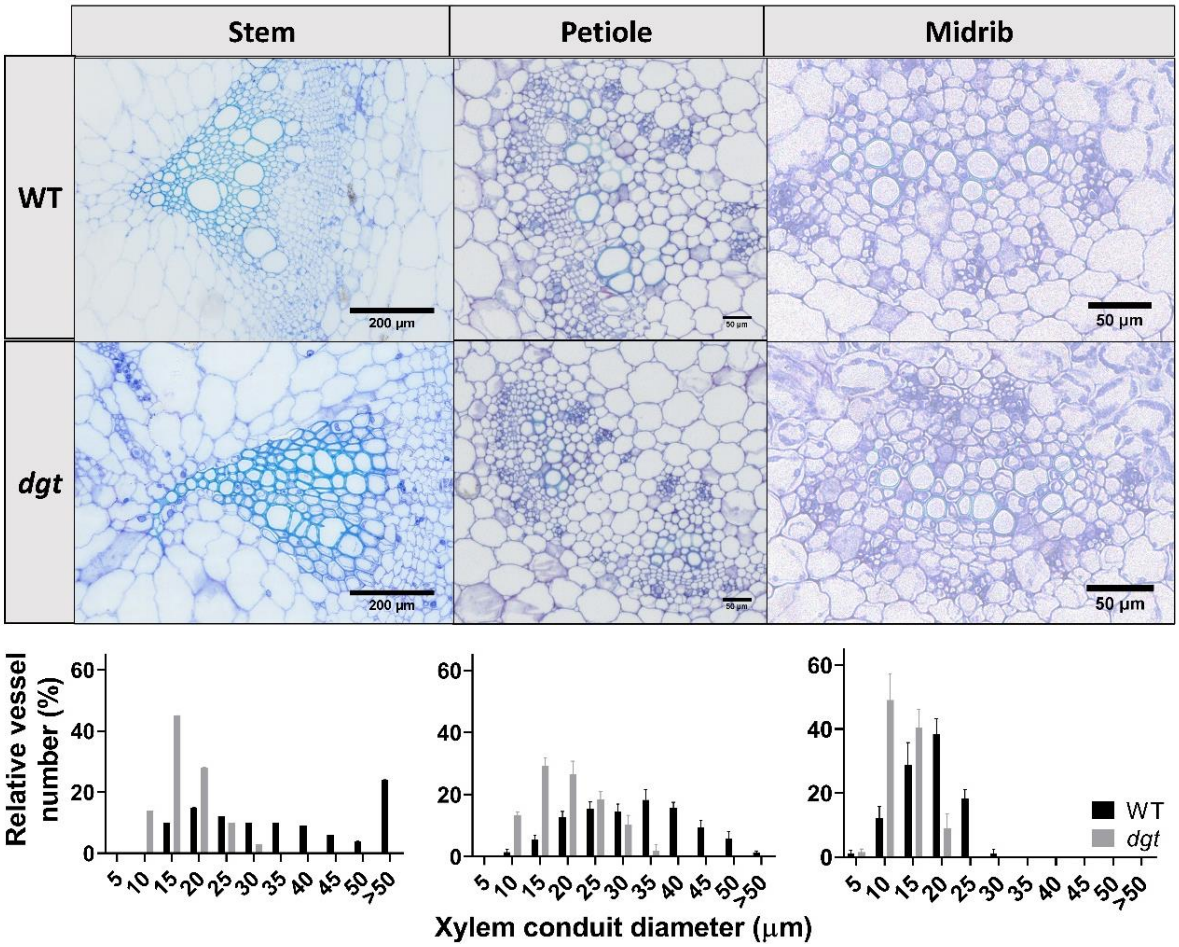

Fig S1. Representative cross-sectional images of stem, petiole, and midrib of tomato from the two genotypes, i.e. WT and *dgt* mutant. The graphs show the relative vessel number (%) per diameter class (µm).

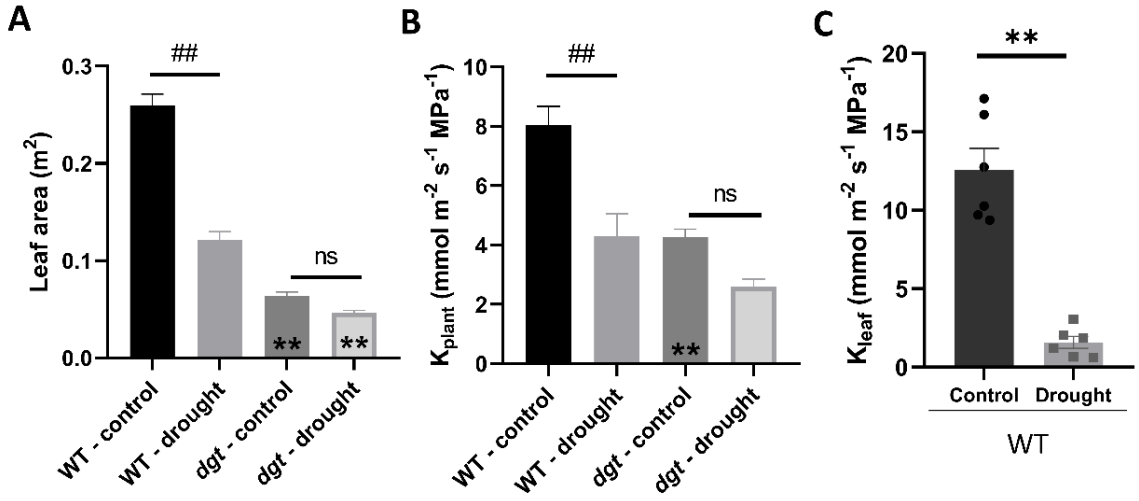

Fig S2. (A) Plant total leaf area and (B) plant hydraulic conductivity of tomato from the two genotypes, i.e. WT and *dgt* mutant, under well-watered conditions (control) and withholding irrigation (water deficit). (C) Leaf hydraulic conductance of WT genotype under control conditions and submitted to *dgt*'s Ψ_{50} (Water deficit).

GENERAL CONCLUSION

In summary, our study shows the first in-depth hydraulic characterization of plants with the impaired auxin signaling mediated by *DGT*. We found considerable changes in xylem anatomy, i.e., reduction in conduits number and diameter (in stems, petiole, and midribs), which resulted in severe impacts on hydraulic efficiency at the whole-plant level. Higher $(t/b)^3$ without major modifications in the pit membranes and cell wall reinforcement makes *dgt* an excellent model to verify the isolated effects of changes in these parameters on cavitation vulnerability. In particular, our analysis identified the roots as the hydraulic bottleneck of *dgt* which was associated with the impairment of secondary root primordium initiation shown by this genotype. Despite the increases in D_v and D_s, which would theoretically increase A_n, A_n was still lower in *dgt*, likely due to a limited water transport capacity. The changes in xylem architecture also resulted in a more negative Ψ_{50}, indicating a possible advantage over WT in a water-limited condition. Indeed, WT plants did not show photosynthetic recovery when submitted to a more intense water deficit (equivalent to Ψ_{50} - 0.25MPa = *dgt*'s Ψ_{50}), confirming the increased hydraulic safety of the *dgt* mutant. Also, we found evidence that *DGT*, an auxin response mediator, plays a relevant role in proper xylem conduit development with strong implications on hydraulic efficiency and safety. Our study shows that the understanding of the nature of the auxin-hydraulic relation might be a pathway to crop improvements in face of environmental changes.